

T.C.

MARMARA UNIVERSITY

INSTITUTE FOR GRADUATE STUDIES IN

PURE AND APPLIED SCIENCES

**STRUCTURAL AND MAGNETIC PROPERTIES OF Co
DOPED ZnO FILMS**

Münevver ÇAKIROĞLU

THESIS

FOR THE DEGREE OF MASTER OF SCIENCE

IN

METALLURGICAL AND MATERIALS ENGINEERING

SUPERVISORS

Assist. Prof. Dr. Seval GENÇ

Assist. Prof. Dr. Lütfi ARDA

T.C.
MARMARA UNIVERSITY
INSTITUTE FOR GRADUATE STUDIES IN
PURE AND APPLIED SCIENCES

**STRUCTURAL AND MAGNETIC PROPERTIES OF Co
DOPED ZnO FILMS**

Münevver ÇAKIROĞLU

(141103520050004)

THESIS

FOR THE DEGREE OF MASTER OF SCIENCE

IN

METALLURGICAL AND MATERIALS ENGINEERING

SUPERVISORS

Assist. Prof. Dr. Seval GENC

Assist. Prof. Dr. Lütfi ARDA

İSTANBUL 2008

ACKNOWLEDGEMENT

I would like to begin thanking to my advisors; Dr.Seval Genc and Dr.Lütfi Arda. I am grateful them for all their help, interests and discussions. This project was made possible with all their help and patience.

I would like to acknowledge Marmara University, Department of Metallurgical and Materials Engineering and Bahçeşehir University, Faculty of Arts and Science.

Special thanks to my husband, Serkan, for his support, help and for his love.

Finally, I would like to thank my father İlhan, my mother Nermin and my sister Merve for their patience and encouragement throughout my study.

November, 2008

Münevver Çakıroğlu

CONTENTS

	PAGE
ACKNOWLEDGEMENT	i
CONTENTS	ii
ÖZET	v
ABSTRACT	vi
FIGURES	vii
TABLES	ix
PART I	1
I.I. INTRODUCTION AND AIM	1
PART II. GENERAL BACKGROUND	2
II.1.MAGNETIC MATERIALS	2
II.2. TYPES OF MAGNETIC MATERIALS	3
II.2.1. Theory of Diamagnetism	3
II.2.2. Theory of Paramagnetism	4
II.2.3. Ordered Magnetic Materials	4
II.2.3.1. Ferromagnetism	4
II.2.3.2. Antiferromagnetism	5
II.2.3.3. Ferrimagnetism	5
II.3. DILUTE MAGNETIC SEMICONDUCTORS	5

II.3.1. Natural Ferromagnetic Semiconductors	6
II.3.2. II-IV Ferromagnetic DMS.....	6
II.3.3. III-V Ferromagnetic DMS.....	9
II.3.4. Co Doped ZnO magnetic Semiconductors	10
II.3.5. Spintronics.....	11
II.4. SOL-GEL PROCESS.....	11
II.5. X-RAY DIFFRACTION.....	13
II.5.1. Properties of x-rays.....	13
II.5.2. Analysis by X-ray Diffraction.....	14
II.6. SCANNING ELECTRON MICROSCOPY (SEM).....	15
II.6.1. Scanning Process and Image Formation.....	16
II.6.2. Sample Preparation.....	17
II.6.3. Energy Dispersive Spectrometer.....	17
II.7. ATOMIC FORCE MICROSCOPE (AFM).....	18
II.7.1. Basic Principles of AFM.....	18
II.7.2. Advantages and Disadvantages of AFM.....	19
PART III. THE STUDY.....	21
III.1. EXPERIMENTAL PROCEDURE.....	20
PART IV. RESULTS AND DISCUSSION.....	29
PART V. CONCLUDING REMARKS AND RECOMMANDATIONS.....	40
REFERENCES.....	41

BIBLIOGRAPY.....

45

ÖZET

Co KATKILI ZnO FİMLERİN YAPISAL VE MANYETİK ÖZELLİKLERİNİN İNCELENMESİ

Co katkıli ZnO filmlerin ve toz numunesinin yapısal ve manyetik özellikleri çalışılmıştır. $Zn_{(1-x)}Co_{(x)}O$ filmler ve toz numuneler, sol-gel yöntemi ile hazırlanmıştır.

$Zn_{(1-x)}Co_{(x)}O$ ince filmleri, cam altlık üzerine sol-gel daldırma yöntemi kullanılarak üretilmiştir. Yapısal karakterizasyon; x-ray, Atomik Kuvvet Mikroskobu (AFM), Taramalı Elektron Mikroskobu (SEM) ve Enerji Dağılım Spektrometresi (EDS) ölçümleri ile belirlenmiştir. Manyetik ölçümler, Kuantum Design PPMS ile ölçüldü ve manyetik alan filme paralel olarak uygulandı. Manyetik ölçüm sonuçlarına göre 0.25 Co konsantrasyonuna sahip $Zn_{(1-x)}Co_{(x)}O$ filmleri 305K sıcaklıkta ferromanyetik özellik gösterdiler.

ABSTRACT

STRUCTURAL AND MAGNETIC PROPERTIES OF Co DOPED ZnO FILMS

Structural and magnetic properties of cobalt doped ZnO films and powders were studied. $Zn_{(1-x)}Co_{(x)}O$ films and powders were prepared by sol-gel method using solutions of Zn, and Co, based organometallic compounds.

$Zn_{(1-x)}Co_{(x)}O$ thin films were produced on glass substrate by a sol-gel dip coating technique. The surface morphologies and thermal properties of samples were investigated by AFM, SEM, EDS and DTA. The crystal and phase structures of the $Zn_{(1-x)}Co_{(x)}O$ film and powder were characterized using x-ray diffraction (XRD). Magnetic measurements were performed with a Quantum Design PPMS with a magnetic field applied parallel to the film. The analysis of the magnetization measurements indicates that $Zn_{(1-x)}Co_{(x)}O$ films with the Co concentration of 0.25 exhibit ferromagnetism at 305 K. Micrographs of the film revealed pinhole-free, crack-free, smooth and dense microstructures.

LIST OF FIGURES

	PAGE
Figure II.1 Three types of semiconductors: a) Nonmagnetic semiconductor, b) DMS, c) DMS with ferromagnetic order mediated by charge carriers (holes).....	6
Figure II.2. Magnetization-Temperature Curve.....	6
Figure II.3. Hysteresis curve for room temperature for MN doped ZnO.....	7
Figure II.4. Comparison of Curie Temperatures.....	9
Figure II.5. Idea for Diluted Magnetic Semiconductors.....	13
Figure III.1 Flow Chart for the Preparation and Coating of ZnCoO Solution on Glass Substrate.....	22
Figure III.2 The reel-to-reel sol-gel coating system.....	23
Figure IV.1 XRD pattern of Zn _{0.99} Co _{0.01} O powder at 600 °C for 30 min.....	25
Figure IV.2 SEM micrographs of the surface of Zn _{0.95} Co _{0.15} O sample with scale bar of 50 a.....	26
Figure IV.3 SEM micrographs of the surface of Zn _{0.95} Co _{0.15} O sample with scale bar of 0.2µm.....	27
Figure IV.4 Micrographs of the surface of Zn _{0.95} Co _{0.15} O sample with scale bar of 0.1µ.....	28
Figure IV.5. AFM images for ZnCoO sample with two-dimensional image, section profile and three-dimensional image (1-10m).....	29

Figure IV.6. AFM images for ZnCoO sample with two-dimensional image, section profile and three-dimensional image (1-5m).....	30
Figure IV.7. EDS analysis of Zn _{0.95} Co _{0.15} O sample.....	31
Figure IV.8. The hysteresis loop of Zn _(1-x) Co _(x) O samples measured at the room temperature for x-concentration of 0.25 and 6 time coating on glass substrate. Inset shows the magnified loop to indicate the field shift.....	32
Figure IV.9. TG and DTA curve of Zn _{0.95} Co _{0.05} O xerogel powder which were dried at room temperature.....	33

LIST OF TABLES

	PAGE
Table II.1. List of Transition Metal Doped ZnO DMOs.....	11
Table III.1. ZnCoO Solutions.....	22
Table III.2. The detail sol-gel Zn (1-x)Co(x)O thin film parameters.....	23

PART I

INTRODUCTION AND AIM

I.1. INTRODUCTOIN AND AIM

The dilute magnetic semiconductors (DMS) were formed by doping small amount of magnetic transition metals (Cr, Ni, Mn, Co, Fe) into the ZnO which is a direct band-gap semiconductor, and showed ferromagnetism with a Curie temperature above room temperature. DMS have attracted much attention because of their promising technological applications such as, reader heads of magnetic hard disk drives, giant magnetic resistance (GMR). Many researchers have worked on it to produce single crystal, film, and bulk forms. They observed different magnetic behaviors of transition metal doped ZnO by using different methods. Regarding these observation, the ferromagnetism strongly depends on the growth condition. These methods include chemical vapour deposition (CVD), pulsed laser deposition, molecular beam epitaxy, rf sputtering, and sol-gel method. Among these methods the sol-gel methods have advantages such as continuous processing at room temperature, better homogeneity, inexpensive method, low cost, and simplicity.

The goals of the present work are: to investigate processing, characterization and sol-gel parameters such as solution properties, withdrawal speed, drying, heat treatment, annealing condition with varying Co doped ratio of the $Zn_{(1-x)}Co_{(x)}O$ films on glass substrate using sol-gel coating techniques; to grow crack free, pinhole-free, uniform $Zn_{(1-x)}Co_{(x)}O$ thin films; to investigate doping ratios and film thicknesses on magnetic properties of thin films.

PART II

II. GENERAL BACKGROUND

II.1. MAGNETIC MATERIALS

Magnetism is an open interdisciplinary field in which physicists, electrical engineers, materials scientists, chemists, metallurgists, and others practice together. Today, information technologies ranging from personal computers to main frames use magnetic materials to store information on tapes, floppy diskettes, and hard disks. Personal computers and many of our consumer and industrial electronics components are now powered largely by lightweight switch-mode power supplies using new magnetic materials technology that was unavailable 20 years ago. Magnetic materials touch many other aspects of our lives. Each automobile contains dozens of motors, actuators, sensors, inductors, and other electromagnetic and magneto mechanical components using hard as well as soft magnetic materials. Electric power generation, transformation, and distribution systems rely on hundreds of millions of transformers and generators that use various magnetic materials ranging from the standard alloys to new amorphous magnetic alloys [1].

The magnetic properties of materials arise almost exclusively from the motion of the electrons. This motion, in the form of electron spin and electron orbital motion, generates a magnetic moment associated with the electron. Much weaker magnetic moments arise from the nucleus, but these are three orders of magnitude smaller [2].

There are two theories on the origin of magnetization or bulk magnetic moment in solids which represent limiting or extreme cases. These are localized or atomic theory, and the itinerant or band theory. In the localized model, the electronic magnetic moments are considered to be bound to the ionic cores in the solid. Such a model applies to the lanthanide series of elements in which the ‘magnetic’ electrons are inner 4f electrons which are closely bound to the nuclei [2].

In band theory, the magnetic moments are considered to be due to conduction band electrons which originate as the outer electrons on the isolated atoms. When the atoms are brought together, as in a solid, these electrons are shared among the atoms and move freely throughout the material. This model is considered by some authors to be more appropriate for the 3d transition elements iron, cobalt, and nickel. In reality, even in the 3d series metals the itinerant electrons spend more time close to the nuclei, and so the actual situation is somewhere between the extreme or limiting models [2].

II.2. TYPES OF MAGNETIC MATERIALS

There are several different types of magnetic materials but it can be separated into three traditional categories; diamagnets, paramagnets, and ordered magnetic materials such as ferromagnets.

This categorization is rather an oversimplification of the different types of magnetic ordering but is still used in magnetism texts. The ordered magnetic materials consist of several subcategories which include: ferromagnets, ferrimagnets, superparamagnets, and even other subcategories with low permeabilities, the antiferromagnets and helimagnets [2].

II.2.1. Theory of Diamagnetism

These are materials which have no net magnetic moment on their atoms. In other words, the electrons are all paired with spins antiparallels. When a magnetic field is applied, the orbits of the electrons change in accordance with Lenz's law, and they set up an orbital magnetic moment which opposes the field. Since this moment is in the opposite direction to the field in diamagnets the susceptibility is negative [2].

II.2.2. Theory of Paramagnetism

Paramagnets are materials which have a net magnetic moment per atom due to an unpaired electron spin. In zero fields these individual magnetic moments are randomly aligned, but under the action of an external field they can be aligned in the field direction. As a result of this alignment of moments in the field direction the magnetization is parallel to the field and hence the susceptibility is positive [2].

II.2.3. Ordered Magnetic Materials

The third class of magnetic materials is the most interesting. These are the ordered magnetic materials, the most important of which are the **ferromagnets**. These include iron, cobalt, and nickel and their alloys and compounds, and several of the rare earth elements, notably gadolinium, and their alloys and compounds [2].

II.2.3.1. Ferromagnetism

Ferromagnetic materials are characterized by a long-range ordering of their atomic moments, even in the absence of an external field. The spontaneous, long-range magnetization of a ferromagnet is observed to vanish above an ordering temperature called the Curie temperature [1].

Permanent magnetic moments in ferromagnetic materials result from atomic magnetic moments due to electron spin, uncancelled electron spins as a consequence of the electron structure. There is also an orbital magnetic moment contribution that is small in comparison to the spin moment. Furthermore, in a ferromagnetic material, coupling interaction causes net spin magnetic moments of adjacent atoms to align with one another, even in the absence of an external field. The maximum possible magnetization, or saturation magnetization, of a ferromagnetic material represents the magnetization that results when all the magnetic dipoles in a solid piece are mutually aligned with the external field; there is also a corresponding saturation flux density [3].

II.2.3.2. Antiferromagnetism

This phenomenon of magnetic moment coupling between adjacent atoms or ions occurs in materials other than those that are **ferromagnetic**. In one such group, coupling results in an antiparallel alignment; the alignment of the spin moments of neighboring atoms or ions in exactly opposite directions is termed **antiferromagnetism**. Manganese oxide is one material that displays this behavior [4]. The theory of antiferromagnetism was developed chiefly by Neel in a series of papers, beginning in 1932 in which he applied the Weiss molecular field theory to the problem. Theory and experiment have been reviewed by Lidiard, Nagamiya, and finally goes through a maximum at a critical temperature called the Neel temperature. The substance is paramagnetic above Neel temperature and antiferromagnetic below it. Neel temperature commonly lies far below room temperature, so that it is often necessary to carry susceptibility measurements down to quite low temperatures to discover if a given substance, paramagnetic at room temperature, is actually antiferromagnetic at some lower temperature [4].

II.2.3.3. Ferrimagnetism

Some ceramics also exhibit a permanent magnetization, termed **ferrimagnetism**. The macroscopic magnetic characteristics of ferromagnets and ferrimagnets are similar; the distinction lies in the source of the net magnetic moments. The saturation magnetizations for ferromagnetic materials are not as high as for ferromagnets. On the other, ferrites, being ceramic materials, are good electrical insulators. For some magnetic applications, such as high-frequency transformers, a low electrical conductivity is most desirable [3].

II.3. DILUTE MAGNETIC SEMICONDUCTORS

The possibility of using electrons' spins in addition to their charge in information technology has created much enthusiasm for a new field of electronics popularly known as spintronics. An intensely studied approach to obtaining spin-polarized carriers for data storage devices is the use of DMSs created by doping ions

like Mn, Fe or Co having a net spin into a semiconducting host such as GaAs, ZnO or GaN. The interaction among these spins leads to ferromagnetic order at low temperatures, which is necessary to create spin-polarized carriers, as it is illustrated in **Figure II.1** [5].

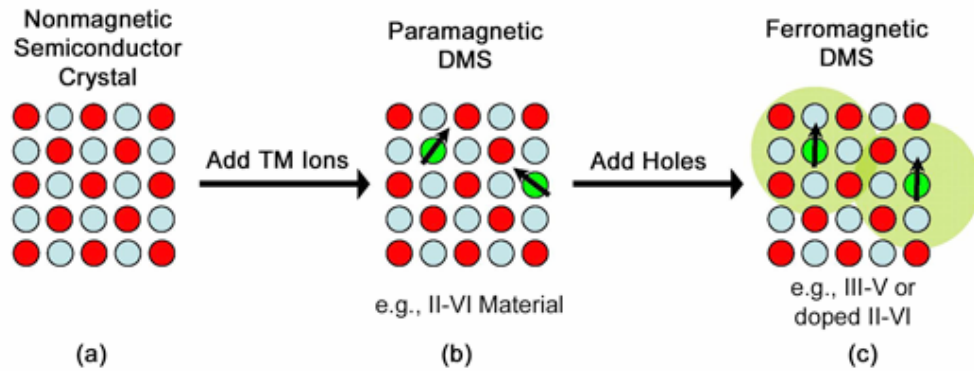


Figure II.1. Types of semiconductors: a) Nonmagnetic semiconductor, b) DMS, c) DMS with ferromagnetic order mediated by charge carriers (holes).

A systematic study of DMSs and their applications in spintronics devices was stimulated by discovery of ferromagnetism in the Mn-doped III-V semiconductors (In, Mn)As and (Ga, Mn)As; shown in **Figure II.2** [5,6,7].

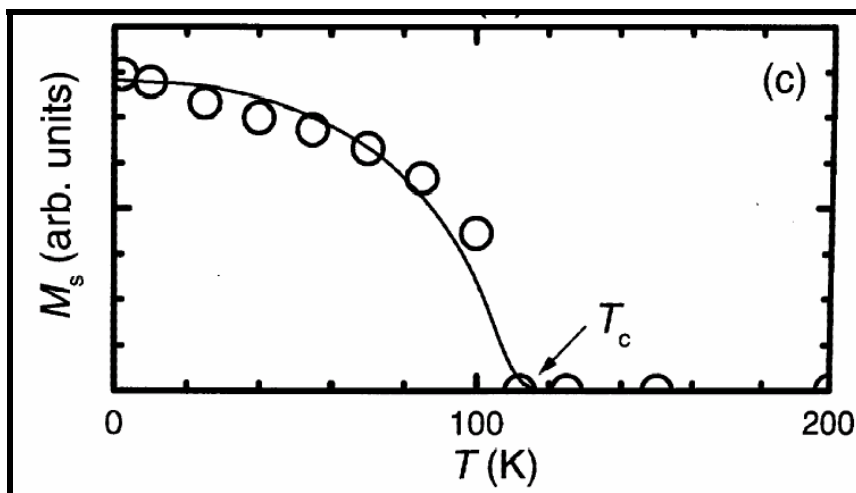


Figure II.2. Magnetization-Temperature Curve

Research on diluted magnetic semiconductors (DMS) has generated great interest for their potential application of semiconductors-based magnetic elements.

Ferromagnetic semiconductors simultaneously exhibit semiconducting properties and spontaneous long range ferromagnetic materials order [8]. The local structures of Mn atoms in ZnO which is shown in **Figure II.3** have been investigated by extended x-ray absorption fine structure. The local structures and magnetic properties of epitaxial ZnO films have been studied [9].

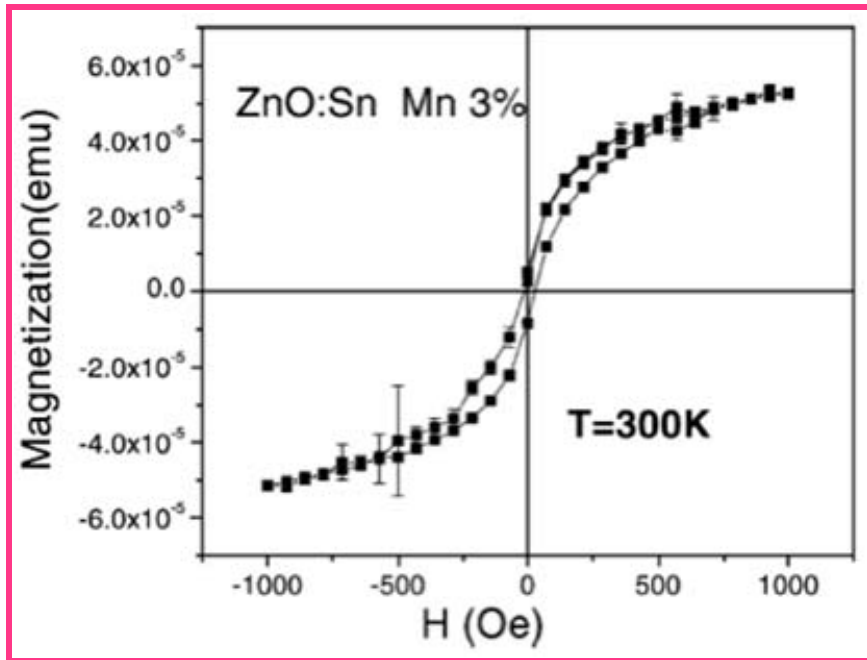


Figure II.3. Hysteresis curve for room temperature for MN doped ZnO

The principal goal in the field of ferromagnetic semiconductors for devices is the synthesis, characterization, and utilization of semiconductors that exhibit substantial carrier spin polarization at and above room temperature. Such materials are of critical importance in the emerging field of semiconductor spintronics [10]. The resulting macroscopic magnetic properties are diverse and critically dependent on growth and processing conditions [11, 12].

II.3.1. Natural Ferromagnetic Semiconductors

There exist a few but rare semiconducting ferromagnets gifted to us by Mother Nature. The search of such material started by a cardinal law of Nature (or may be

due to law of large numbers) that anything that is theoretically not impossible should exist [13]. Ferromagnetism and semiconducting properties coexist in magnetic semiconductors, such as europium chalcogenides and semiconducting spinels that have a periodic array of magnetic elements. In these magnetic semiconductors, which were extensively studied in the late 1960s to early 1970s, exchange interactions between the electrons in the semiconducting band and the localized electrons at the magnetic ions lead to a number of peculiar and interesting properties, such as a red shift of band gap when ferromagnetism sets in. Unfortunately, the crystal structure of such magnetic semiconductors is quite different from that of Si and GaAs; in addition, the crystal growth of these compounds is notoriously difficult. To obtain even a small, single crystal requires weeks of preparation and growth [13].

II.3.2. II-IV Ferromagnetic DMS

The usefulness of semiconductors resides in the ability to dope them with impurities to change their properties, usually to p- or n-type. This approach can be followed to introduce magnetic elements into nonmagnetic semiconductors to make them magnetic. These categories of semiconductors, called diluted magnetic semiconductors (DMSs), are alloys of nonmagnetic semiconductor and magnetic elements. Study of DMSs and their heterostructures have centered mostly on II-VI semiconductors, such as CdTe and ZnSe, in which the valence of the cations matches that of the common magnetic ions such as Mn. Although this phenomenon makes these DMSs relatively easy to prepare in bulk form as well as in thin epitaxial layers, II-VI based DMSs have been difficult to dope to create p and n-type, which made the material less attractive for applications [13].

Moreover, the magnetic interaction in II-VI DMSs is dominated by the antiferromagnetic, exchanges among the Mn spins, which results in the paramagnetic, antiferromagnetic, or spin glass behavior of the material [13].

II.3.3. III-V Ferromagnetic DMS

An approach compatible with the semiconductors used in present-day electronics is to make nonmagnetic III-V semiconductors magnetic, and even

ferromagnetic, by introducing a high concentration of magnetic ions. The II-V semiconductors such as GaAs which is shown in **Figure II.4** are already in use in a wide variety of electronic equipment in the form of electronic and optoelectronic devices, including cellular phones (microwave transistors), compact disks (semiconductor lasers), and in many other applications. Therefore, the introduction of magnetic III-V semiconductors opens up the possibility of using a variety of magnetic phenomena not present in conventional nonmagnetic III-V semiconductors in the optical and electrical devices already established [13]. The major obstacle in making III-V semiconductors magnetic has been the low solubility of magnetic elements (such as Mn) in the compounds. Because the magnetic effects are roughly proportional to the concentration of the magnetic ions, one would not expect a major change in properties with limited solubility of magnetic impurities, of the order of 10^{18} cm^{-3} or less. A breakthrough was made by using molecular beam epitaxy (MBE), a thin-film growth technique in vacuum that allows one to work far from equilibrium. When a high concentration of magnetic elements is introduced in excess of the solubility limit, formation of the second phase occurs if conditions are near equilibrium. However, when the crystal is grown at low temperature by MBE, there is not enough thermal energy available to form the second phase, and yet there still exists a local potential landscape that allows epitaxial growth of a single-crystal alloy. The effort to grow new III-V based DMSs by low-temperature MBE was rewarded with successful epitaxial growth of uniform (In, Mn)As films on GaAs substrates in 1989, where partial ferromagnetic order was found, and ferromagnetic (Ga, Mn)As in 1996 [14-20].

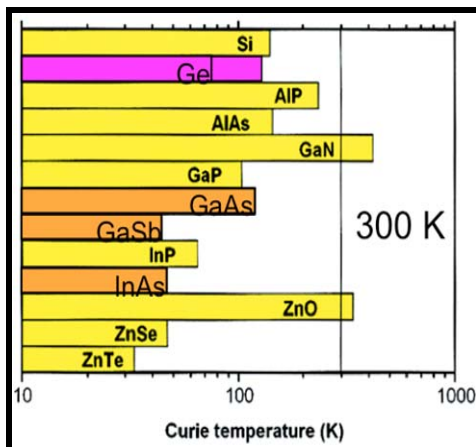


Figure II.4. Comparison of Curie Temperatures

II.3.4. Co-doped ZnO Magnetic Semiconductors

Wide band gap semiconductors such as GaN and ZnO have been identified as promising DMS materials as they exhibit ferromagnetism at room temperature and are optically transparent to visible light. From the opto and magneto electronics applications point of view ZnO is attractive because of high exciton energy = 60 meV and band gap=3.3 eV.

Incorporation of substitutional TM ions in II-VI ZnO should be less difficult than incorporating them in other semiconductor hosts, since the valence of Zn (2^+) and the ionic radius can be readily adopted by many 3d TM ions [14]. **Table II.1**, shows a list of Co-doped ZnO DMOs, including the substrate, T_c , TM content and the corresponding magnetization features at 300K [21].

It is evident from Table II.1 that Co-doped ZnO is the most popular system in the literature, not only because of its thermal solubility in ZnO films, but also because of their high magnetic moments at room temperature [21].

Table II.1. List of Transition Metal Doped ZnO DMOs

System	TM Content (at.%)	Substrate	T _c (K)	Magnetization Features
Co:ZnO	5 (5-25)	Al ₂ O ₃	>280	0.01 μB/Co
Co:ZnO	25	Al ₂ O ₃	-	Spin Glass
Co:ZnO	3.5 (3.5-11.5)	Glass	>350	0.21 μB/Co
Co:ZnO	5	Al ₂ O ₃	300	0.7 μB/mole Co
Co:ZnO	25	Al ₂ O ₃	>300	1.0 μB/Co
Co:ZnO	35	Al ₂ O ₃	>300	0.1 μB/Co
Co:ZnO	7 (7-17)	Si	>300	0.06 μB/Co
Co:ZnO	10	Al ₂ O ₃	>300	0.00005 emu
Co:ZnO	5	Al ₂ O ₃	>300	2.6 μB/Co
Co:ZnO	25	Al ₂ O ₃	300	0.8 μB/Co
Co:ZnO	1.3 (0-5)	Al ₂ O ₃	>300	0.32 μB/Co
Co:ZnO	5	Si	>300	1.04 μB/Co
Co:ZnO	0.3-0.5	Al ₂ O ₃	>300	3 μB/Co
Co:ZnO	2	Si	>300	0.4 μB/Co
Co:ZnO	3 (1-25)	Al ₂ O ₃	>300	5.9 μB/Co
Co:ZnO	4	LiNbO ₃	790	6.1 μB/Co
Co:ZnO	5	ZnO/Al ₂ O ₃	>300	1.5 μB/Co
Co:ZnO	2 (2-13)	Al ₂ O ₃	>300	0.8 μB/Co
Co:ZnO	12 (8-31)	Al ₂ O ₃	>300	0.04 μB/Co
Co:ZnO	10	ZnO	-	antiferromagnetism
Co:ZnO	5	Si	>300	0.5 μB/Co

Magnetic and structural studies of Cobalt doped ZnO were studied by many scientists. The polycrystalline bulk samples with nominal composition were studied by the standard solid state method. It is observed that the structure and magnetic properties of samples were dependent on doping concentration [22]. In other work, doping of ZnO bulk ceramics with small amounts of tin oxide was studied on samples prepared by a highly reactive co-precipitation method. Better results should be expected in the form of thin film device [23].

Another example was studied about the synthesis of nanocrystalline powders of Co-doped ZnO diluted magnetic semiconductor by a simple method using acetate salts of Zn and Co, and polyvinyl pyrrolidone as precursors [24]. The X-ray diffraction and Transmission Electron Microscopy (TEM) results indicated that the

synthesized ZCO powders had the pure wurtzite structure without any significant change in the structure affected by Co substitution [24]. Co-workers, Ueda, Tabata and Kawai studied magnetic and electric properties of transition-metal-doped ZnO films. The Co-doped ZnO films showed the maximum solubility limit. Some of them exhibit ferromagnetic behaviors with the Curie temperature higher than room temperature [25]. In another study, Mn-doped ZnO samples were studied [26]. Epitaxial thin films of an oxide-diluted magnetic semiconductor, Mn-doped ZnO, were fabricated by pulsed-laser deposition technique. It was seen that, the large in-gap absorption may open up an optically controlled magnetism in such a transparent oxide-diluted magnetic semiconductor [26]. Progress in wide band gap ferromagnetic semiconductors and the role of defects and doping on the resulting magnetic properties were studied by Pearton and co-workers. They used the theory which predicts a Curie temperature greater than 300 K for p-type GaN and ZnO, with Curie temperature dependent on the concentration of magnetic ions and holes [27].

Co-workers; Tiwari, Jin, Kvit, Kumar, Muth, and Narayan studied structural properties of diluted magnetic semiconducting ZnMnO films. They prepared high quality epitaxial ZnMnO films on sphere using a pulsed laser deposition technique [28]. A systematic study of the structural properties of these high quality epitaxial films showed a 30° rotation of the film with respect to the substrate similar to III-nitride growth on sphere substrate [28]. Doped ZnO films are either conducting or semiconducting, as characterized by strong coupling between localized d electrons of the transition metal (TM) ions and the extended s and p ions carriers of ZnO. Thus the carriers are spin-polarized and can mediate ferromagnetic ordering of the magnetic moments of TM ions doped into the oxide lattice, i.e., TM ions replace Zn^{+2} sites [21].

II.3.5. Spintronics

Spintronics devices manipulate current with charge and spin. This added degree of control will require materials that have magnetic properties in addition to the traditional electronic properties [21]. The idea of spintronics can be seen in the **Figure II.5;**

Motivation

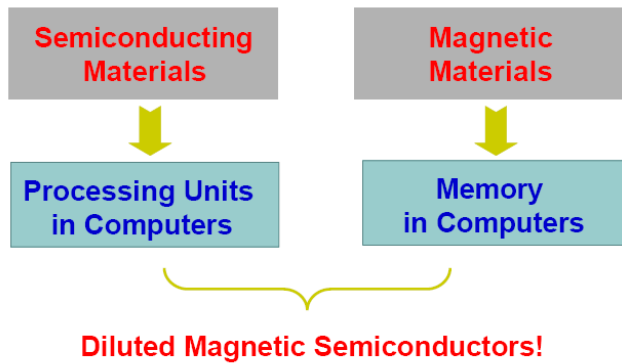


Figure II.5. Idea for Diluted Magnetic Semiconductors.

II.4. SOL-GEL PROCESS

Sol-gel processing is chemical synthesis of oxides involving hydrolysable alkoxides that undergo a sol-gel transition. This definition is often interpreted to mean any system that undergoes a sol-gel transition, including colloidal sols and soluble salts. Nevertheless the majority of systems investigated in the last ten years fit the narrow definition that the sol-gel transition represents a linking of nanometer-sized units into an oxide network of infinite molecular weight [7].

Sol-gel processing has been used to prepare glasses, glass-ceramics, and ceramics. Either amorphous and crystalline materials can result depending on the composition, the precursors, the handling, and heat treatments. These factors lead to either a powder process or a powder-free process. A powder process refers to any process that uses discrete particles, which in this case are generated from a sol-gel process. A powder-free process refers to any process that does not involve an aggregation of discrete particles. Starting from hydrolysable alkoxides, a powder-free process would generate a porous perform of a glass or ceramic in the desired geometry may be a thin film, a fiber, or a bulk shape called a monolith. The sol-gel technique offers many advantages over other methods, such as; low temperature processing, precise control of doping level and simplicity [7].

An alternative approach to glass and glass-like materials is offered by the, so called, sol-gel technology. The process itself is known for more than a century, but it has gained a new importance in the last two decades after pioneering results of Dislich. He and other researchers improved the chemistry of the process so much that it is now possible to obtain samples in days rather than months like in the case of the early samples [29].

The sol-gel technique is based on hydrolysis of liquid precursors and formation of colloidal sols. The precursors are usually organosilicates like tetraethoxysilane (TEOS) yielding silicate sol-gel materials. However, the method is not restricted to the silicon compounds, like compounds of zirconium, vanadium, etc. can be used as precursors leading to materials possessing different physico-chemical properties. Furthermore, it is possible to obtain modified organosilicates precursors with direct Si-C bonds and possessing terminal functional groups. Such precursors, either pure or mixed with the conventional ones, yield inorganic-organic materials with mechanical and physico-chemical properties modified by the organic components of the inorganic polymer network. The functional groups can be also used for covalent binding of various chemicals, including biomolecules, giving specifically modified glassy materials [29].

In the case of the most often employed silicate sol-gel matrices, manufactured from hydrolizates of various alkoxysilanes, the chemical reactions involved in the gel formation involve the precursor hydrolysis: and the subsequent formation of the silicate network. At this stage a wet gel is produced which, upon drying, yields porous xerogels. The drying is accompanied by liquid expulsion from the pores and substantial matrix shrinkage often leading to cracks. The hydrolysis process is significantly improved. Thus, addition of acid or base speeds up this process. After the hydrolysis the acidity of the sol is neutralized slowly. At this stage a mechanically unstable "wet" gel is formed. Drying of wet gels (even at ambient temperatures) leads to xerogels ("dry gels"). Xerogels are stable, transparent and insoluble in water and most of organic solvents and porous solid materials. In cases when fully-densified sol-gel glasses are sought, extensive drying at temperatures close to the vitrification temperatures will yield such materials. This enables

obtaining glasses in situations when it is not feasible via the conventional melting techniques [29].

Since the early steps of the sol-gel process occur in liquid phase, it is possible to add basically any substance (as solutions or suspensions) at this stage. Simple mixing provides uniform distribution of the dopant within the liquid host phase. After the gelation the guest molecules become physically entrapped within the now solid host matrix. Furthermore, the hydrolysis, doping and gelation occur usually at ambient temperatures, allowing entrapment of even such delicate molecules as proteins without their decomposition. Sol-gel doped matrices, obtained in the above described manner, are of the form of xerogels and possess a network of internal pores and cavities enabling the entrapped molecules to interact with the surrounding medium. Furthermore, the doped matrices usually possess good optical characteristics. Those features are of key importance for production of optical sensors [29].

II.5. X-RAY DIFFRACTION

II.5.1. Properties of x-rays

X-rays were discovered in 1895 by the German physicist Roentgen and were so named because their nature was unknown at the time. Unlike ordinary light, these rays were invisible, but they travelled in straight lines and affected photographic film in the same way as light. On the other hand, they were much more penetrating than light and could easily pass through the human body, wood, quite thin pieces of metal and other opaque objects [30].

It is not always necessary to understand a thing in order to use it and x-rays were almost immediately put to use by physicians and, somewhat later, by engineers, who wished to study the internal structure of opaque materials. By placing a source of x-rays on one side of the object and photographic film on the other, a shadow picture or radiograph, could be made, the less dense portions of the object allowing a greater proportion of the x-radiation to pass through than the denser. In this way the

point of fracture in a broken bone or the position of a crack in a metal casting could be easily located [30].

Radiography was thus initiated without any precise understanding of the radiation used because it was not until 1912 that the exact nature of x-rays was established. In that year the phenomenon of x-ray diffraction by crystals was discovered and this discovery simultaneously proved the wave nature of x-rays. This provided a new method for investigating the fine structure of the matter. Although radiography is a very important tool in itself and has a wide field of applicability, it is ordinarily limited in the internal detail it can resolve or disclose, to sizes of the order of 10^{-1} cm. Diffraction, on the other hand, can indirectly reveal details of internal structure of the order of 10^{-8} cm in size, and it is with this phenomenon and its applications to metallurgical problems [30].

II.5.2. Analysis by X-ray Diffraction

A given substance always produces a characteristic diffraction pattern, whether that substance is present in pure state or as one constituent of a mixture of substances. This fact is the basis for the diffraction method of chemical analysis. Qualitative analysis for a particular substance is accomplished by identification of the pattern of that substance. Qualitative analysis is also possible, because the intensities of the diffraction lines due to one phase of a mixture depend on the proportion of that phase in the specimen [30].

The particular advantage of diffraction analysis is that it discloses the presence of a substance as that substance actually exists in the sample and not in terms of its constituent chemical elements. Diffraction analysis is useful whenever it is necessary to know the state of chemical combination of the elements involved or the particular phases in which they are present. Diffraction method has been widely applied for the analysis of such materials as ores, clays, refractory materials, alloys, corrosion products, coated products, wear products and industrial dusts [30].

II.6. SCANNING ELECTRON MICROSCOPY (SEM)

The scanning electron microscope (SEM) is a type of electron microscope that images the sample surface by scanning it with a high-energy beam of electrons in a raster scan pattern. The electrons interact with the atoms that make up the sample producing signals that contain information about the sample's surface topography, composition and other properties such as electrical conductivity. This particular type of microscope is exceedingly useful [31].

The types of signals made by an SEM can include secondary electrons, back scattered electrons, characteristic x-rays and light. These signals come from the beam of electrons striking the surface of the specimen and interacting with the sample at or near its surface. In its primary detection mode, secondary electron imaging, the SEM can produce very high-resolution images of a sample surface, revealing details about 1 to 5 nm in size. Due to the way these images are created, SEM micrographs have a very large depth of focus yielding a characteristic three-dimensional appearance useful for understanding the surface structure of a sample. This great depth of field and the wide range of magnifications are available in the most common imaging mode for specimens in the SEM, secondary electron imaging, such as the micrograph taken of pollen shown to the right. Characteristic x-rays are the second most common imaging mode for an SEM. X-rays are emitted when the electron beam removes an inner shell electron from the sample, causing a higher energy electron to fill the shell and give off energy. These characteristic x-rays are used to identify the elemental composition of the sample. Back-scattered electrons (BSE) that come from the sample may also be used to form an image. BSE images are often used in analytical SEM along with the spectra made from the characteristic x-rays as clues to the elemental composition of the sample [31]

II.6.1. Scanning Process and Image Formation

In a typical SEM, electrons are thermionically emitted from a tungsten filament cathode and are accelerated towards an anode. Tungsten is normally used in thermionic electron guns because it has the highest melting point and lowest vapour

pressure of all metals, thereby allowing it to be heated for electron emission. Other electron sources include lanthanum hexaboride (LaB6) cathodes, which can be used in a standard tungsten filament SEM if the vacuum system is upgraded. Electrons can also be emitted using a field emission gun (FEG), which may be of the cold-cathode type or the thermally-assisted Schottky type [31].

The electron beam is focused by one or two condenser lenses into a beam with a very fine focal spot sized 0.4 nm to 5 nm. The beam passes through pairs of scanning coils or pairs of deflector plates in the electron column, typically in the final lens, which deflect the beam horizontally and vertically so that it scans in a raster fashion over a rectangular area of the sample surface [31].

When the primary electron beam interacts with the sample, the electrons lose energy by repeated scattering and absorption within a teardrop-shaped volume of the specimen known as the interaction volume, which extends from less than 100 nm to around 5 μm into the surface. The size of the interaction volume depends on the electron's landing energy, the atomic number of the specimen and the specimen's density. The energy exchange between the electron beam and the sample results in the reflection of high-energy electrons by elastic scattering, emission of secondary electrons by inelastic scattering and the emission of electromagnetic radiation which can be detected to produce an image [31].

Electronic devices are used to detect and amplify the signals and display them as an image on a cathode ray tube in which the raster scanning is synchronized with that of the microscope. The image displayed is therefore a distribution map of the intensity of the signal being emitted from the scanned area of the specimen. The image may be captured by photography from a high resolution cathode ray tube, but in modern machines is digitally captured and displayed on a computer monitor [31].

II.6.2. Sample Preparation

Because the SEM utilizes vacuum conditions and uses electrons to form an image, special preparations must be done to the sample. All water must be removed from the samples because the water would vaporize in the vacuum. All metals are

conductive and require no preparation before being used. All non-metals need to be made conductive by covering the sample with a thin layer of conductive material. This is done by using a device called a "sputter coater" [32].

The sputter coater uses an electric field and argon gas. The sample is placed in a small chamber that is at a vacuum. Argon gas and an electric field cause an electron to be removed from the argon, making the atoms positively charged. The argon ions then become attracted to a negatively charged gold foil. The argon ions knock gold atoms from the surface of the gold foil. These gold atoms fall and settle onto the surface of the sample producing a thin gold coating [32].

II.6.3. Energy Dispersive Spectrometer

Chemical analysis (microanalysis) in the scanning electron microscope (SEM) is performed by measuring the energy or wavelength and intensity distribution of X-ray signal generated by a focused electron beam on the specimen. With the attachment of the energy dispersive spectrometer (EDS) or wavelength dispersive spectrometers (WDS), the precise elemental composition of materials can be obtained with high spatial resolution. When we work with bulk specimens in the SEM very precise accurate chemical analyses (relative error 1-2%) can be obtained from larger areas of the solid (0.5-3 micrometer diameter) using a n EDS or WDS. Bellow is an example of EDS spectrum collected in the SEM with EDS. The spectrum shows presence of Al, Si, Ca, Mn and Fe in the steel slag phase [32].

II.7. ATOMIC FORCE MICROSCOPE (AFM)

The **atomic force microscope** (AFM) or scanning force microscope (SFM) is a very high-resolution type of scanning probe microscope, with demonstrated resolution of fractions of a nanometer, more than 1000 times better than the optical diffraction limit. The precursor to the AFM, the scanning tunneling microscope, was developed by Gerd Binnig and Heinrich Rohrer in the early 1980s, a development that earned them the Nobel Prize for Physics in 1986. Binnig, Quate and Gerber

invented the first AFM in 1986. The AFM is one of the foremost tools for imaging, measuring and manipulating matter at the nanoscale. The term 'microscope' in the name is actually a misnomer because it implies looking, while in fact the information is gathered by "feeling" the surface with a mechanical probe. Piezoelectric elements that facilitate tiny but accurate and precise movements on command are what facilitate the very precise scanning [32].

II.7.1. Basic Principles of AFM

The AFM consists of a microscale cantilever with a sharp tip (probe) at its end that is used to scan the specimen surface. The cantilever is typically silicon or silicon nitride with a tip radius of curvature on the order of nanometers. When the tip is brought into proximity of a sample surface, forces between the tip and the sample lead to a deflection of the cantilever according to Hooke's law. Depending on the situation, forces that are measured in AFM include mechanical contact force, Van der Waals forces, capillary forces, chemical bonding, electrostatic forces, magnetic forces and solvation forces. As well as force, additional quantities may simultaneously be measured through the use of specialized types of probe. Typically, the deflection is measured using a laser spot reflected from the top of the cantilever into an array of photodiodes. Other methods that are used include optical interferometry, capacitive sensing or piezoresistive AFM cantilevers. These cantilevers are fabricated with piezoresistive elements that act as a strain gauge. Using a Wheatstone bridge, strain in the AFM cantilever due to deflection can be measured, but this method is not as sensitive as laser deflection or interferometry [32].

If the tip were scanned at a constant height, there would be a risk that the tip would collide with the surface, causing damage. Hence, in most cases a feedback mechanism is employed to adjust the tip-to-sample distance to maintain a constant force between the tip and the sample. Traditionally, the sample is mounted on a piezoelectric tube that can move the sample in the z direction for maintaining a constant force, and the x and y directions for scanning the sample. Alternatively a 'tripod' configuration of three piezo crystals may be employed, with each responsible

for scanning in the x, y and z directions. This eliminates some of the distortion effects seen with a tube scanner. The resulting map of the area represents the topography of the sample [32].

II.7.2. Advantages and Disadvantages of AFM

The AFM has several advantages over the scanning electron microscope (SEM). Unlike the electron microscope which provides a two-dimensional projection or a two-dimensional image of a sample, the AFM provides a true three-dimensional surface profile. Additionally, samples viewed by AFM do not require any special treatments that would irreversibly change or damage the sample. While an electron microscope needs an expensive vacuum environment for proper operation, most AFM modes can work perfectly well in ambient air or even a liquid environment. This makes it possible to study biological macromolecules and even living organisms. In principle, AFM can provide higher resolution than SEM [32].

A disadvantage of AFM compared with the scanning electron microscope (SEM) is the image size. The SEM can image an area on the order of millimeters by millimeters with a depth of field on the order of millimeters. The AFM can only image a maximum height on the order of micrometers and a maximum scanning area of around 150 by 150 micrometers [32].

Another inconvenience is that an incorrect choice of tip for the required resolution can lead to image artifacts. Traditionally the AFM could not scan images as fast as an SEM, requiring several minutes for a typical scan, while an SEM is capable of scanning at near real-time after the chamber is evacuated. The relatively slow rate of scanning during AFM imaging often leads to thermal drift in the image, making the AFM microscope less suited for measuring accurate distances between artifacts on the image. However, several fast-acting designs were suggested to increase microscope scanning productivity including what is being termed video AFM. To eliminate image distortions induced by therm drift [32].

AFM images can also be affected by hysteresis of the piezoelectric material and cross-talk between the axes that may require software enhancement and filtering.

Such filtering could "flatten" out real topographical features. However, newer AFM use real-time correction software or closed-loop scanners which practically eliminate these problems. Some AFM also use separated orthogonal scanners which also serve to eliminate cross-talk problems [32].

PART III

III. THE STUDY

III.1. EXPERIMENTAL PROCEDURE

The system $Zn_{(1-x)}Co_xO$ was prepared as solutions and polycrystalline nano powders with various compositions ($0.01 \leq x \leq 0.3$) by applying the sol-gel technique. Zinc acetate dihydrate (Fluka), Cobalt acetate (Merck) was used as precursor materials. Methanol, isopropanol, 2-methoxyethanol and acetyl acetone were used as solvents and chelating agent. In order to improve adhesion of $Zn_{(1-x)}Co_xO$ on the glass substrates, triethanolamine (TEA), diethanolamine (DEA) and monoethanolamine (MEA) were used. Before preparation of the solutions, the precursors were weighted out by using a standard balance. The Zn and Co compounds were dissolved in 100 ml flasks using solvents and chelating agents as listed in **Table III.1** and then stirred with a magnetic stirrer for 8 hours at room temperature until transparent solution was obtained. Moreover, triethanolamine (TEA), diethanolamine (DEA) and monoethanolamine (MEA) were used. in the solution.

Finally, thirteen of variety ZnCoO solutions were prepared, pH values of the transparent solutions were measured carefully to determine their acidic and basis characteristic using a standard pH meter.

Figure III.1 shows flow chart for the preparation of ZnCoO coatings on glass substrate. Glass substrates were cleaned in pure acetone and distilled water by using ultrasonic cleaner, respectively. ZnCoO films were grown on glass substrate using sol-gel dip-coating technique at a varying withdrawal speed **Table III.1**. **Figure III.2** shows the system of sol-gel coating. Furnace temperature was 300-400 °C. Process was repeated various times in order to achieve dense and homogeneous coating. After completing the coating process $Zn_{1-x}Co_xO$ /glass films were annealed

at a varying temperature and for varying time under air in a box furnace as shown in **Table III.2**.

X-ray diffraction profiles of powder samples and coated films were recorded using Rigaku diffractometer with Cu K- α radiation. Data for powder and coated samples were collected at a room temperature over the range between $20 < 2\theta < 80$ in 0.02 step, with an integration time of 0.5 seconds. Surface morphology, thickness and stoichiometry of coating films were observed by using Scanning Electron Microscope (SEM, Jeol 5919LV), the Energy Dispersive Spectroscopy (EDS) and Atomic Force Microscope (AFM).

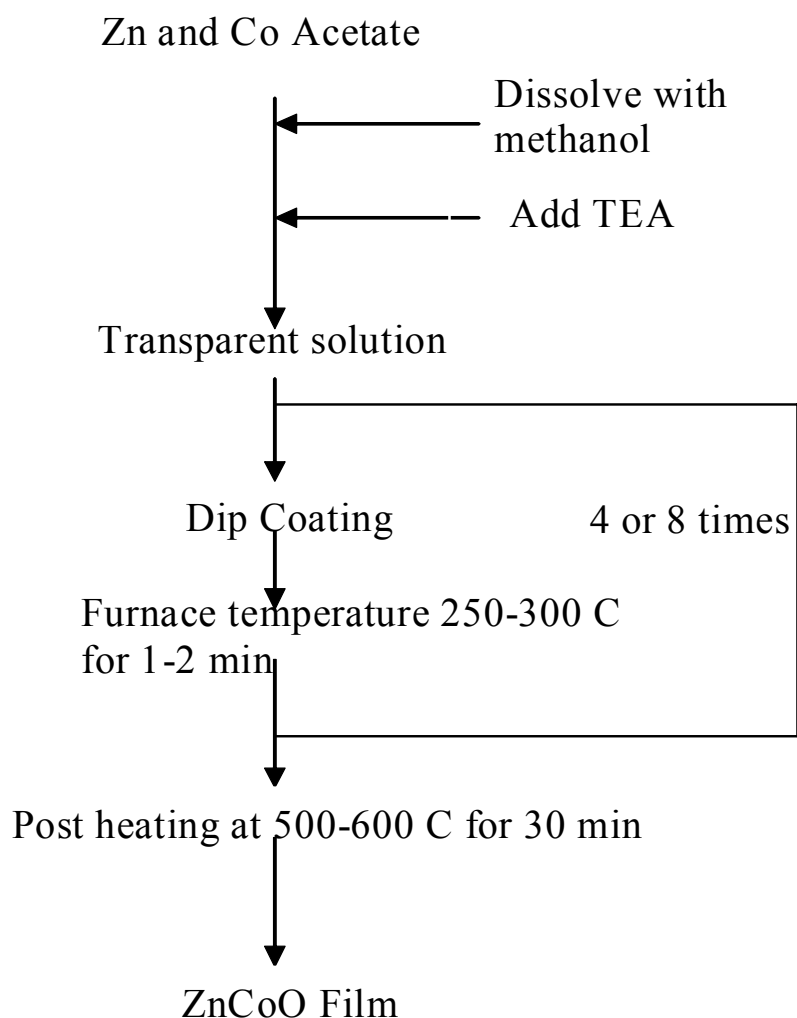


Figure III.1. Flow chart for the preparation and coating of ZnCoO solution on glass substrate

Table III.1 ZnCoO Solutions

Solutions	Used chemical materials
ZnCoO(1)	Zinc acetate dehydrate, Cobalt acetate, methanol, acetyl acetone, triethanolamine
ZnCoO(2)	Zinc acetate dehydrate, Cobalt acetate, isoproponal, acetyl acetone, triethanolamine
ZnCoO(3)	Zinc acetate dehydrate, Cobalt acetate, isoproponal, triethanolamine
ZnCoO(4)	Zinc acetate dehydrate, Cobalt acetate, isoproponal, monoethanolamine
ZnCoO(5)	Zinc acetate dehydrate, Cobalt acetate, methanol, acetyl acetone, monoethanolamine
ZnCoO(6)	Zinc acetate dehydrate, Cobalt acetate, methanol, triethanolamine
ZnCoO(7)	Zinc acetate dehydrate, Cobalt acetate, 2-methoxyethanol, monoethanolamine
ZnCoO(8)	Zinc acetate dehydrate, Cobalt acetate, 2-methoxyethanol, diethanolamine
ZnCoO(9)	Zinc acetate dehydrate, Cobalt acetate, 2-methoxyethanol, triethanolamine
ZnCoO(10)	Zinc acetate dehydrate, Cobalt acetate, methanol, diethanolamine
ZnCoO(11)	Zinc acetate dehydrate, Cobalt acetate, isoproponal, diethanolamine
ZnCoO(12)	Zinc acetate dehydrate, Cobalt acetate, isoproponal, acetyl acetone, diethanolamine
ZnCoO(13)	Zinc acetate dehydrate, Cobalt acetate, isoproponal, acetyl acetone, monoethanolamine

Table III.2.The detail sol-gel Zn (1-x)Co(x)O thin film parameters

Films	Number of Dip	Vert. Furnace Temp. (C)	Withdrawal speed (m/min)	Post annealing Temp (C)	Time (min)
ZnCoO(1)	4,5,6,7,8,9, 10	250	0.60	600	30
ZnCoO(2)	4,5,6,7,8,9, 10	250	1.2	600	30
ZnCoO(3)	4,5,6,7,8,9, 10	250	1.5	600	30
ZnCoO(4)	4,5,6,7,8,9, 10	250	0.60	600	60
ZnCoO(5)	4,5,6,7,8,9, 10	250	1.2	600	60
ZnCoO(6)	4, ,6,7,8,9, 10	250	1.5	600	60
ZnCoO(7)	4,5,6,7,8,9, 10	250	0.60	600	90
ZnCoO(8)	4,5,6,7,8,9, 10	250	1.2	600	90
ZnCoO(9)	4,5,6,7,8,9, 10	250	1.5	600	90
ZnCoO(10)	4,5,6,7,8,9, 10	300	0.60	600	30
ZnCoO(11)	4,5,6,7,8,9, 10	300	1.2	600	30
ZnCoO(12)	4,5,6,7,8,9, 10	300	1.5	600	30
ZnCoO(13)	4,5,6,7,8,9, 10	300	0.60	600	60
ZnCoO(14)	4,5,6,7,8,9, 10	300	1.2	600	60
ZnCoO(15)	4, ,6,7,8,9, 10	300	1.5	600	60
ZnCoO(16)	4,5,6,7,8,9, 10	300	0.60	600	90
ZnCoO(17)	4,5,6,7,8,9, 10	300	1.2	600	90
ZnCoO(18)	4,5,6,7,8,9, 10	300	1.5	600	90
ZnCoO(19)	4,5,6,7,8,9, 10	350	0.60	600	30
ZnCoO(20)	4,5,6,7,8,9, 10	350	1.2	600	30
ZnCoO(21)	4,5,6,7,8,9, 10	350	1.5	600	30
ZnCoO(22)	4,5,6,7,8,9, 10	350	0.60	600	60
ZnCoO(23)	4,5,6,7,8,9, 10	350	1.2	600	60
ZnCoO(24)	4, ,6,7,8,9, 10	350	1.5	600	60
ZnCoO(25)	4,5,6,7,8,9, 10	350	0.60	600	90
ZnCoO(26)	4,5,6,7,8,9, 10	350	1.2	600	90
ZnCoO(27)	4,5,6,7,8,9, 10	350	1.5	600	90

Table III.2.The detail sol-gel Zn (1-x)Co(x)O thin film parameters(continue)

Films	Number of Dip	Vert. Furnace Temp. (C)	Withdrawal speed (m/min)	Post annealing Temp (C)	Time (min)
ZnCoO(1)	4,5,6,7,8,9, 10	250	0.60	550	30
ZnCoO(2)	4,5,6,7,8,9, 10	250	1.2	550	30
ZnCoO(3)	4,5,6,7,8,9, 10	250	1.5	550	30
ZnCoO(4)	4,5,6,7,8,9, 10	250	0.60	550	60
ZnCoO(5)	4,5,6,7,8,9, 10	250	1.2	550	60
ZnCoO(6)	4, ,6,7,8,9, 10	250	1.5	550	60
ZnCoO(7)	4,5,6,7,8,9, 10	250	0.60	550	90
ZnCoO(8)	4,5,6,7,8,9, 10	250	1.2	550	90
ZnCoO(9)	4,5,6,7,8,9, 10	250	1.5	550	90
ZnCoO(10)	4,5,6,7,8,9, 10	300	0.60	550	30
ZnCoO(11)	4,5,6,7,8,9, 10	300	1.2	550	30
ZnCoO(12)	4,5,6,7,8,9, 10	300	1.5	550	30
ZnCoO(13)	4,5,6,7,8,9, 10	300	0.60	550	60
ZnCoO(14)	4,5,6,7,8,9, 10	300	1.2	550	60
ZnCoO(15)	4, ,6,7,8,9, 10	300	1.5	550	60
ZnCoO(16)	4,5,6,7,8,9, 10	300	0.60	550	90
ZnCoO(17)	4,5,6,7,8,9, 10	300	1.2	550	90
ZnCoO(18)	4,5,6,7,8,9, 10	300	1.5	550	90
ZnCoO(19)	4,5,6,7,8,9, 10	350	0.60	550	30
ZnCoO(20)	4,5,6,7,8,9, 10	350	1.2	550	30
ZnCoO(21)	4,5,6,7,8,9, 10	350	1.5	550	30
ZnCoO(22)	4,5,6,7,8,9, 10	350	0.60	550	60
ZnCoO(23)	4,5,6,7,8,9, 10	350	1.2	550	60
ZnCoO(24)	4, ,6,7,8,9, 10	350	1.5	550	60
ZnCoO(25)	4,5,6,7,8,9, 10	350	0.60	550	90
ZnCoO(26)	4,5,6,7,8,9, 10	350	1.2	550	90
ZnCoO(27)	4,5,6,7,8,9, 10	350	1.5	550	90

Co-doped ZnO magnetic coating was grown on glass substrate using the sol-gel deep coating system as shown in **Fig. III.2**

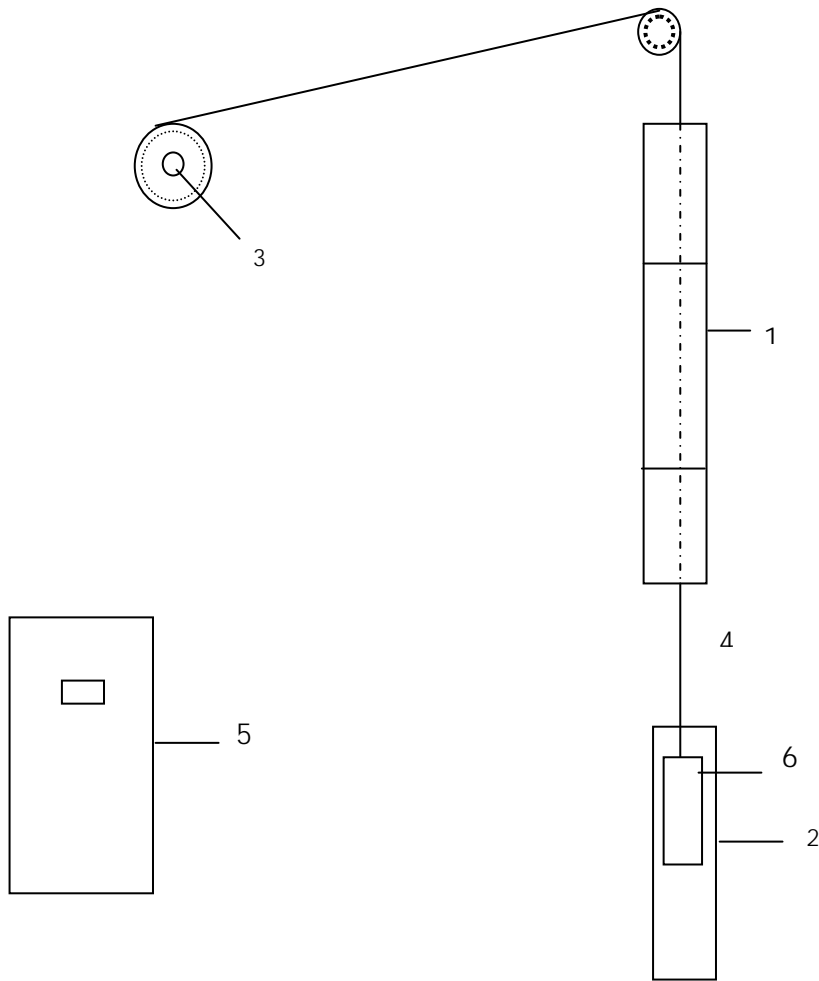


Figure III.2. The reel-to-reel sol gel coating system: (1) a three-zone-furnace, (2) solution container, (3) take-up spool, (4) wire, (5) furnace controllers and (6) substrate.

PART IV

IV. RESULTS AND DISCUSSION

Even though pinhole-free, crack-free, smooth and dense growth of ZnCoO thin films on varying substrate such as glass, Si, Al₂O₃ and LiNbO₃ has been demonstrated by chemical vapour deposition (CVD), pulsed laser deposition, molecular beam epitaxy, rf sputtering, sol-gel method, many papers have been published about structural, magnetic, electric and optical properties of ZnCoO. In this study, we have demonstrated preparation, growth, process, compositions and magnetic properties of ZnCoO on glass substrate by sol-gel process. We discussed preparation, growth and processing condition of the thin films, which depends on solution components, preheating and post annealing conditions such as temperature and time as well as growth and processing condition as well as magnetic properties.

Sol-gel solution components are precursor, solvents, chelating agents and solution modifying chemicals. Two main groups are therefore distinguished a) metallic salts and b) alkoxides. In this study alkoxides based precursor were used. They are Zn acetate dehydrate and Co acetate. Concentration of the ZnCoO thin film solution was adjusted by methanol, isopropanol and 2-methoxyethanol and complexation reaction of Zn and Co acetate precursor was controlled with them. Hydrolyses reaction was controlled by acetyl acetone. Chelation ratios (A) and complexation ratios (B) of sol-gel solution is determined with the equations; IV.1 and IV.2.

$$A = \frac{\sum S}{\sum P} \quad (\text{IV.1}) \quad (\text{IV.1})$$

$$B = \frac{\sum CA}{\sum P} \quad (\text{IV.2}) \quad (\text{IV.2})$$

ΣS : The total amount of solvent; ΣP : total amount of precursor; ΣCA : total amount of chelating agent. All of units are (g).

After using (IV.1) and (IV.2) Equations, various $Zn_{1-x}Co_xO$ with ($0.01 \leq x \leq 0.3$) solutions were prepared to obtain powder samples for crystal structure analysis. After solutions become transparent, solvent were removed at room temperature by using magnetic stirrer and $Zn_{1-x}Co_xO$ powders were obtained. The thermal behaviors of the exogels are analyzed by using DTA and TGA to find the heat treatment temperatures in the zones of furnace. DTA and TG result was shown in page 50. Moreover, various $Zn_{1-x}Co_xO$ with ($0.01 \leq x \leq 0.3$) solutions were prepared to growth $Zn_{1-x}Co_xO$ films on glass substrate by using sol-gel process. It was chosen because of possessing advantages not only processing but also application. The processing advantages are; excellent bonding, thickness of the films (submicron (thin films) to micron (thick film)), thickness can be controlled via solution chemistry, withdrawal rate and number of dipping. The applications advantages are; very attractive low temperature technique, being inexpensive, low cost and simplicity.

Glass substrates were dipped into the solutions (Table III.2) at a withdrawal rate of 0.6, 0.9, 1.2 and 1.5 m/min in the sol-gel set up in Fig. III.2. The gel films were dried and samples were preheated at 250-350°C for 2 min. an in line vertical three zone furnace (Fig. III.2). Process was repeated several times (Table 2) in order to achieve dense and uniform coating at the desired thickness. After that all films were post-annealed at varying temperature for varying time using box furnace. The best post annealing temperature was found at 600°C for 30 min as well as $Zn_{0.75}Co_{0.25}O$ sample which were prepared with 7 dips with dilute solutions were showed best magnetic properties. The quality of magnetic semiconductor film depends on withdrawal speed, drying, heat treatment condition and sol structure such as chemical composition, purity of precursor solvent catalyst materials and pH value of starting and stabilized solution. XRD analysis were used to find phase and crystal structure of the samples. The X-ray diffractions of $Zn_{0.99}Co_{0.01}O$ powder at 600°C for 30 min in the air is shown in **Figure IV.1**.

The peaks that are clearly seen in the XRD pattern belong to the hexagonal ZnO phase (wurtzite). The diffraction peaks along with their relative intensities are found to be in agreement with those from JCPDS. No secondary phase or metallic Co clusters are observed in the pattern which indicates that, the wurtzite structure might have not affected due to the substitution of cobalt. This shows that Co^{+2} is

substituted for Zn^{+2} ions in the ZnO hexagonal lattice since no excess peaks were detected it can be concluded that all the starting organic precursors might have been completely decomposed. The diffraction pattern is in agreement with the patterns reported by other scientist [33- 38].

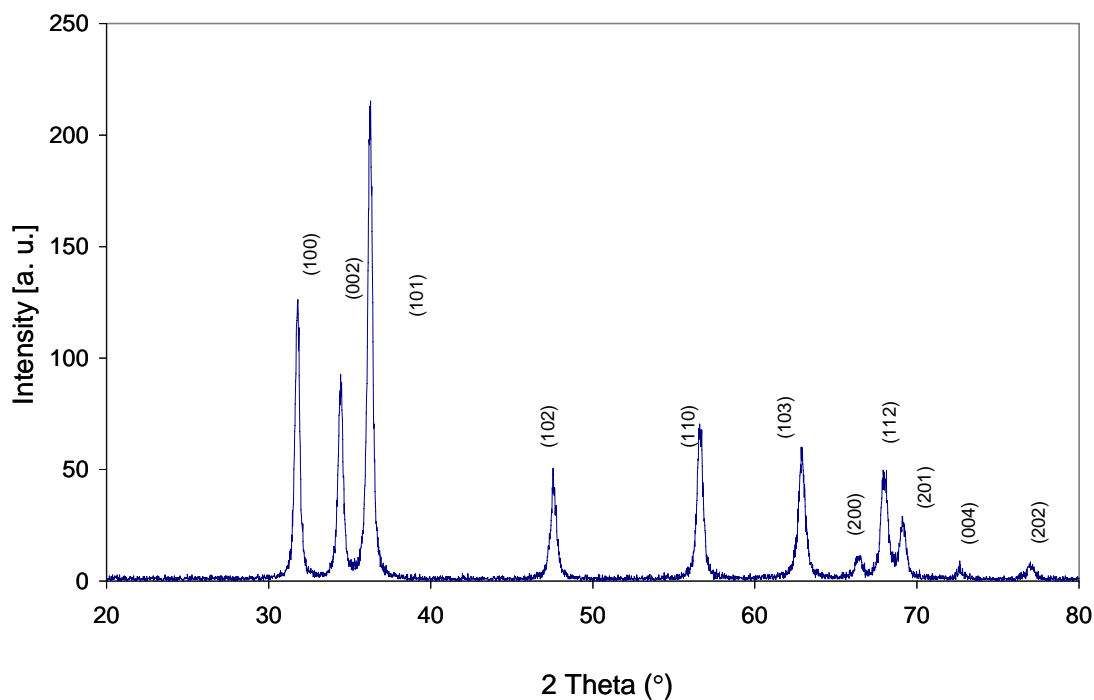


Figure IV.1. XRD pattern of $Zn_{0.99}Co_{0.01}O$ powder at 600 °C for 30 min

Microstructure studies of the ZnCoO films, grown on glass substrate, exhibit a uniform, dense, smooth, and crack-free surface morphology. **Figures IV.2-4** show surface morphologies and SEM micrographs of the ZnCoO structure. SEM images also indicate that there is no secondary phases present.

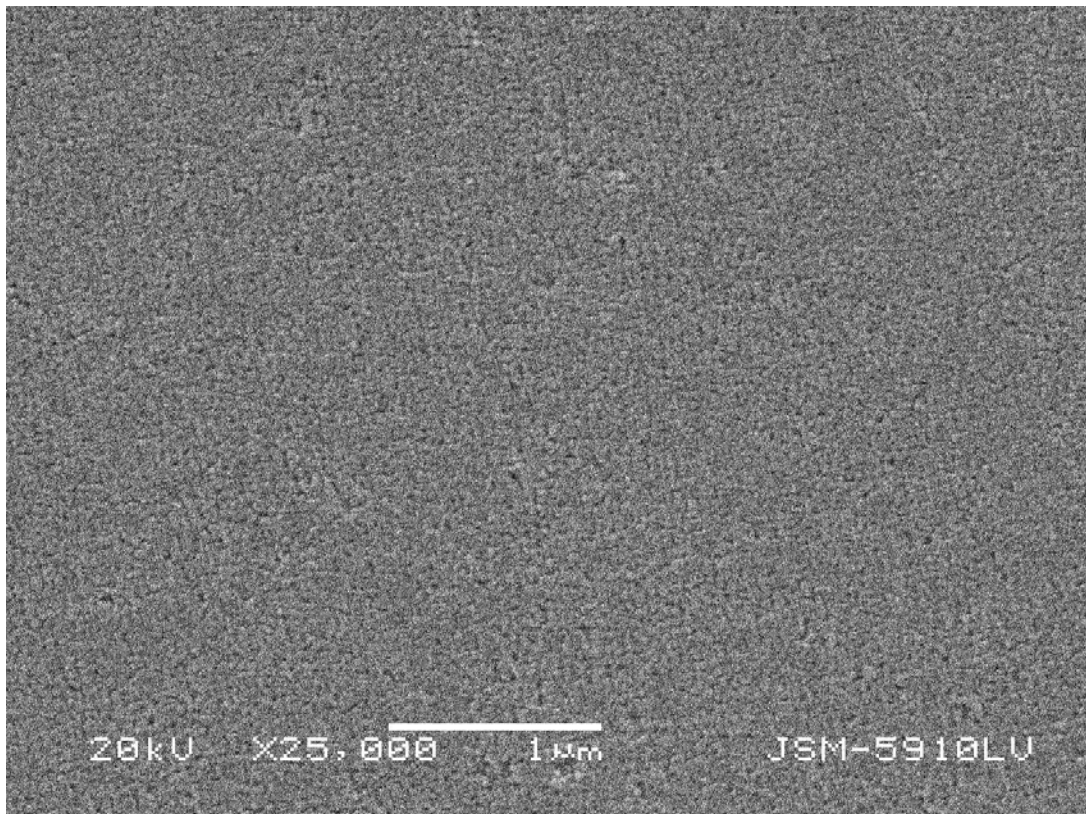
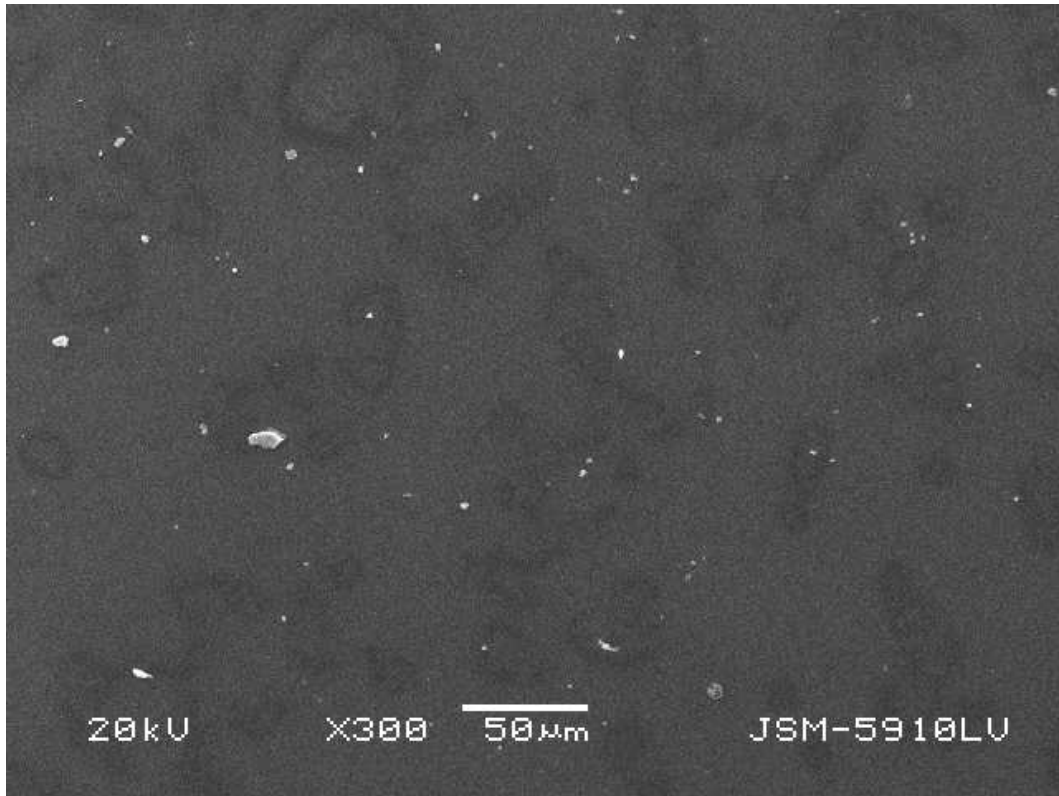


Figure IV. 2 SEM micrographs of the surface of Zn_{0.95}Co_{0.15}O sample with scale bar of 50 and 1 μm

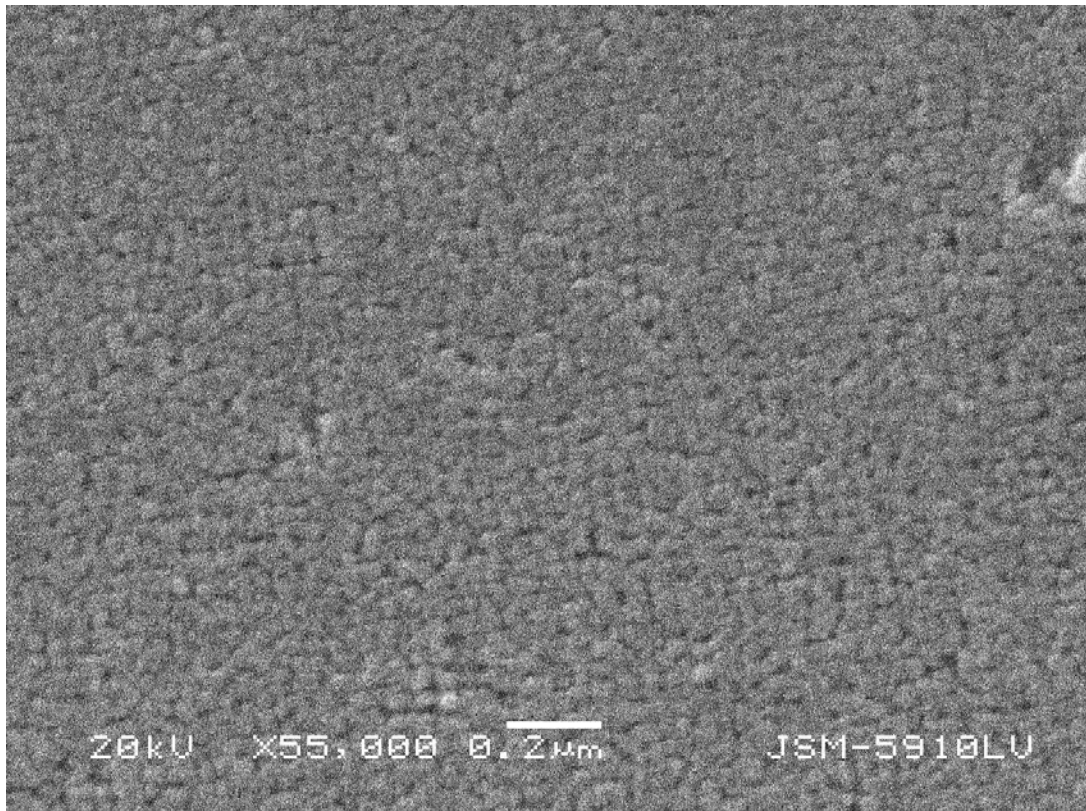
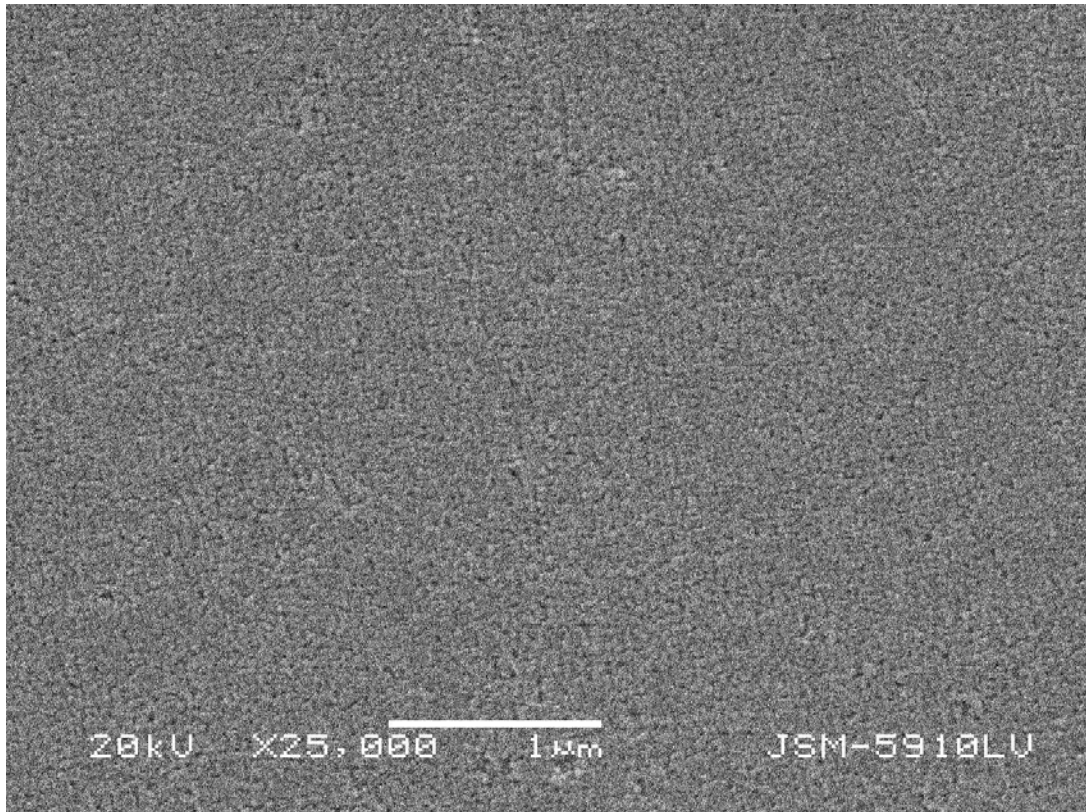


Figure IV. 3. SEM micrographs of the surface of Zn_{0.95}Co_{0.15}O sample with scale bar of 0.2 μm

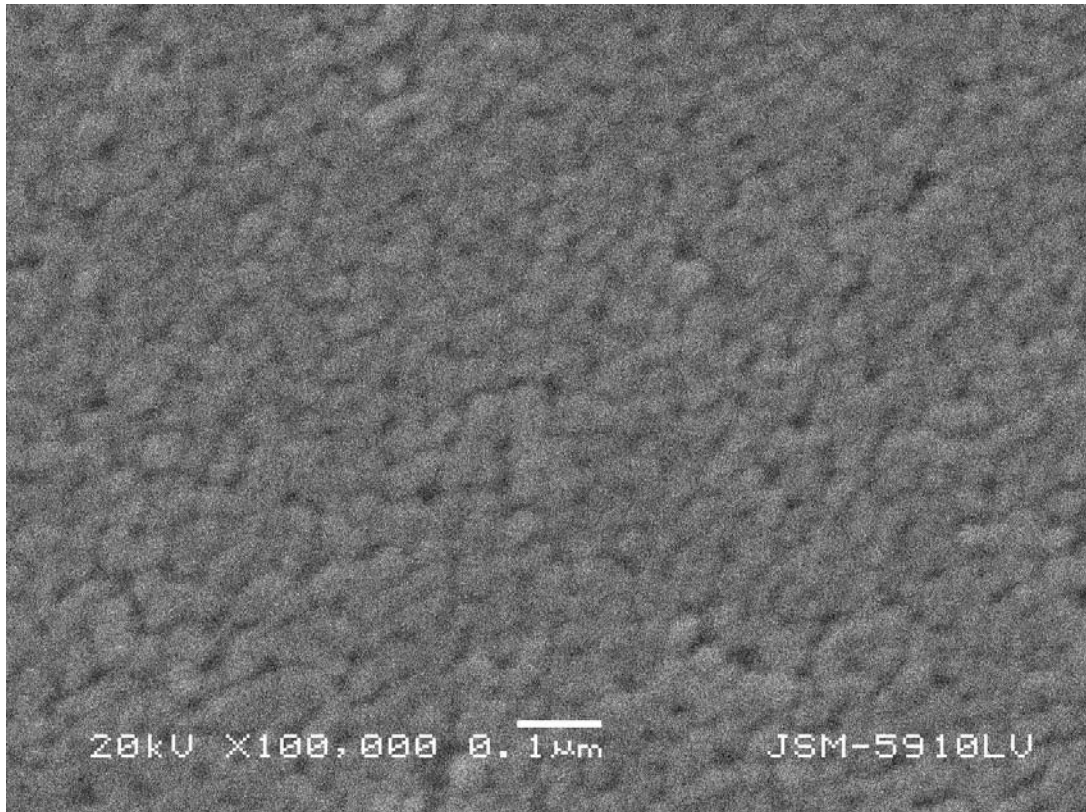


Figure IV. 4. SEM micrographs of the surface of Zn_{0.95}Co_{0.15}O sample with scale bar of 0.1µm

The AFM images obtained on ZnCoO structure is shown in **Figure IV.5** and **Figure IV.6**. As it is seen from the figures smooth samples could be prepared with the sol-gel technique.

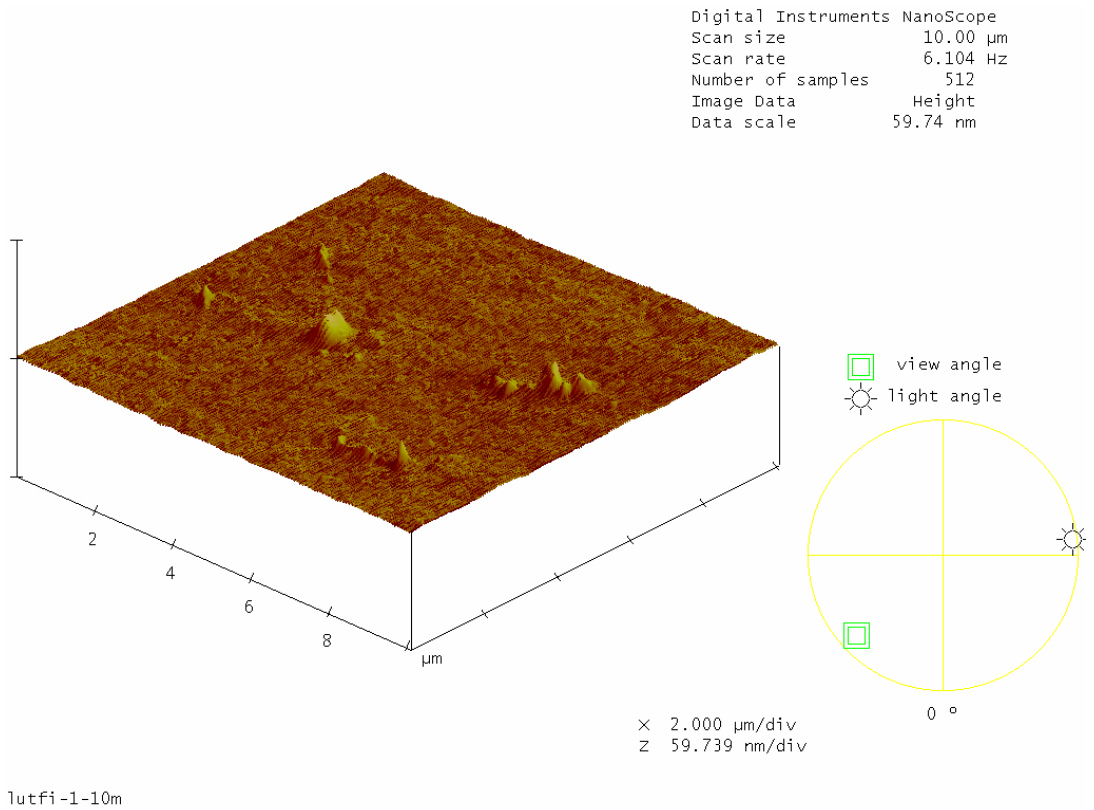
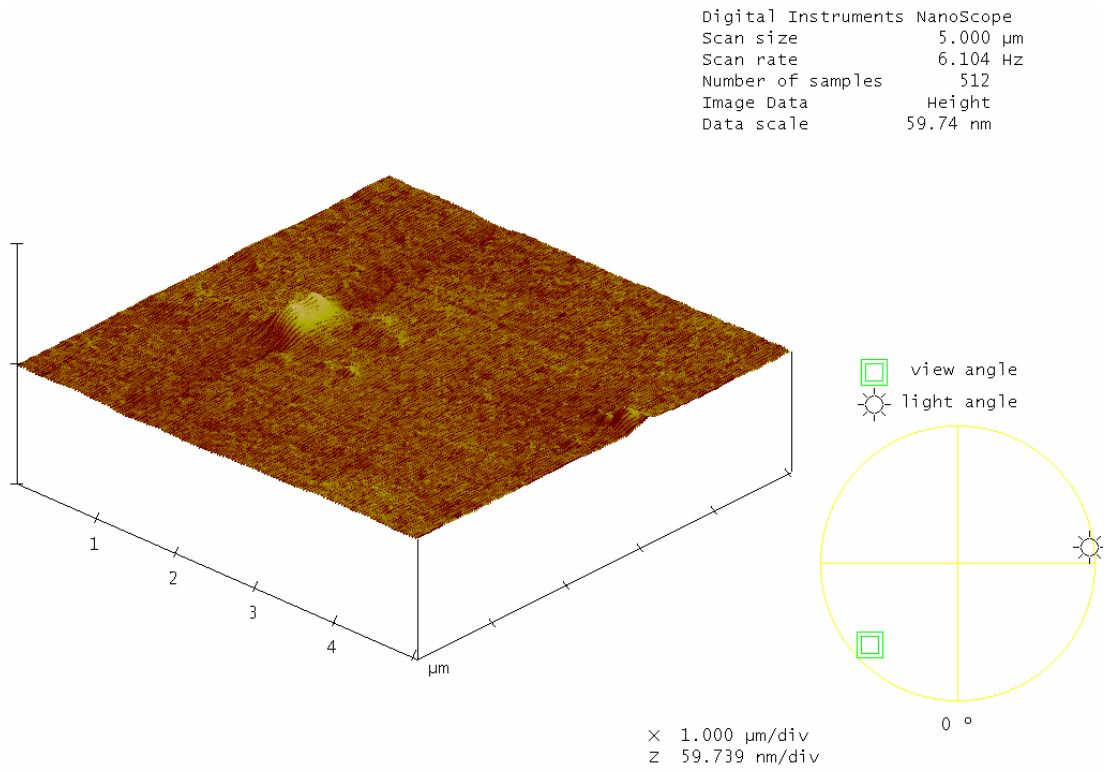


Figure IV.5. AFM images for ZnCoO sample with three-dimensional image (1-10m)



lutfi-1-5m

Figure IV.6. AFM images for ZnCoO sample with three-dimensional image (1-5m)

EDS analysis of the sample $\text{Zn}_{0.95}\text{Co}_{0.15}\text{O}$ is shown in **Figure IV.7**. Zn, Co and O, Si, Al, Mg, Zr, Pd, Ca, Na, Al peaks, belong to coating and substrate, respectively, were observed from spectrum.

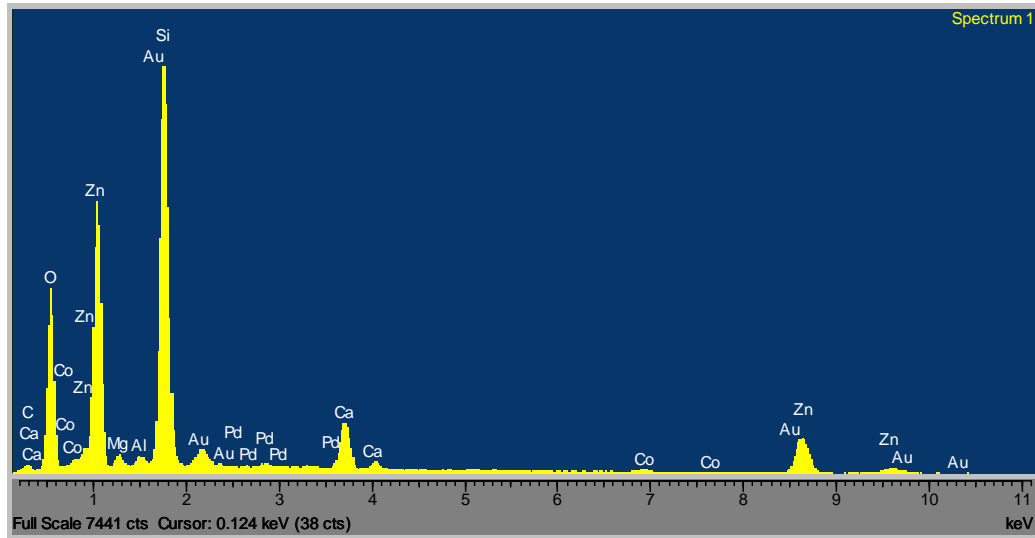


Figure IV.7. EDS analysis of $\text{Zn}_{0.95}\text{Co}_{0.15}\text{O}$ sample

For the measurements of magnetic properties, a Quantum Design physical property measurement system (PPMS) was employed. The applied field dependence of magnetization of $\text{Zn}_{(1-x)}\text{Co}_{(x)}\text{O}$ thin films were recorded by using a VSM magnetometer at 305 K. **Fig.IV.8** shows the magnetization hysteresis loop of the $\text{Zn}_{(1-x)}\text{Co}_{(x)}\text{O}$ for x-concentration of 0.25, as a function of magnetic field which is applied along the film plane, at room temperature. The saturation magnetization of the $\text{Zn}_{(1-x)}\text{Co}_{(x)}\text{O}$ is about 55 emu/cc. As can be seen in the inset of Figure IV.8, hysteresis loop serves a clear field shift of 15 Oe. This result is same as with Ref. [37]

Existence of magnetic ordering in dilute magnetic semiconductors such as ZnCoO is carrier mediated exchange (electron and hole) interaction. The exchange interaction takes place between the holes and electrons as free delocalized carriers and the localized d spin on transition metals. In this study a shift of 15 Oe in the coercive field shows exchange field H_{ex} . This is the most important proof for ferromagnetism [38].

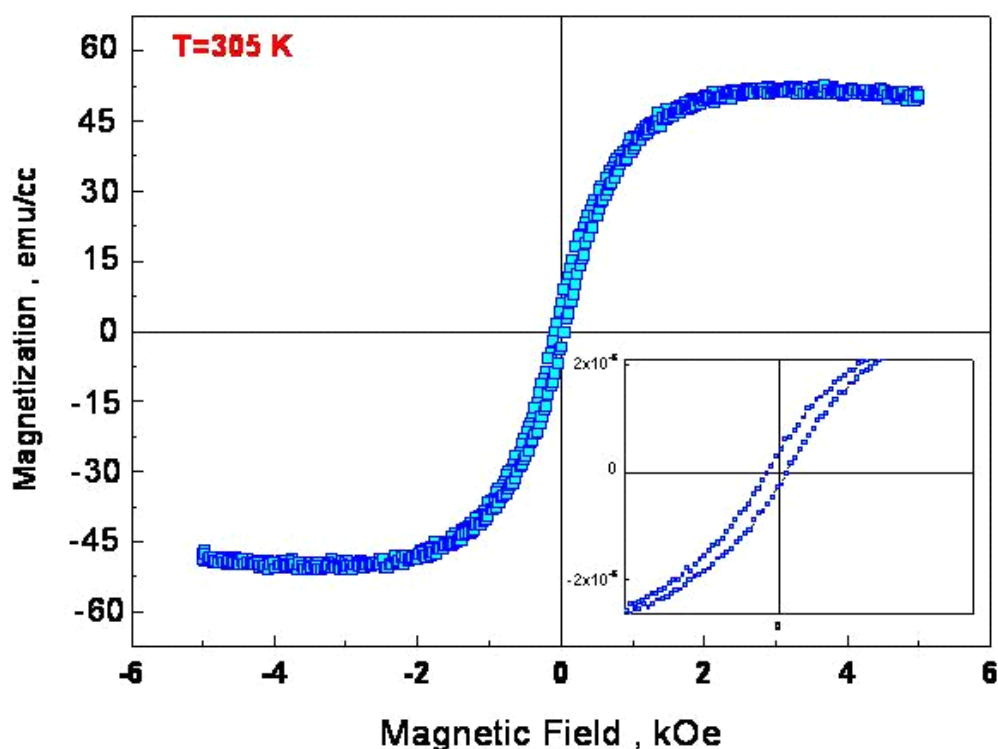


Figure IV.8. The hysteresis loop of Zn_(1-x)Co_(x)O samples measured at the room temperature for x-concentration of 0.25 and 6 time coating on glass substrate. Inset shows the magnified loop to indicate the field shift.

However, the presence of ferromagnetism in ZnCoO films is not yet understood completely. In the study by Belghazi et al, the films that were obtained by spray pyrolysis technique presented a pure paramagnetic contribution and no sign of ferromagnetism [38]. They concluded that no free carriers were available in their system to mediate the magnetic interaction between the magnetic ions as Zn and Co are isovalent.

The thermal behaviour of the xerogels of Zn_{0.95}Co_{0.05}O powder was studied by using differential thermal analysis (DTA) in N(Nitrogen) atmosphere and thermogravimetric analysis techniques.

Figure IV.9 shows the TG chart for the Zn_{0.95}Co_{0.05}O which is obtained by drying the sol-gel solution at room temperature in air for 2 days. The Zn_{0.95}Co_{0.05}O xerogels were analyzed in the temperature range between 20 and 800 °C in air. The first weight decrease due to removal of the solvent and evaporation of volatile

organic component is seen at 100 °C as shown in Figure IV.9. The percentage weight loss was 13.18 %. The carbon-based materials burned out in two steps. First step; the second weight decrease was observed at 100-300 °C. Second step; the third weight decrease was observed at 300-420 °C. The combustion of carbon based materials was completed at 420 °C. The percentage of second and third lost weight was 49.97 %. The oxidation was started around 420 °C and finished around 600 °C. The percentage of fourth weight loss was 2.59 % observed at 500-800 °C.

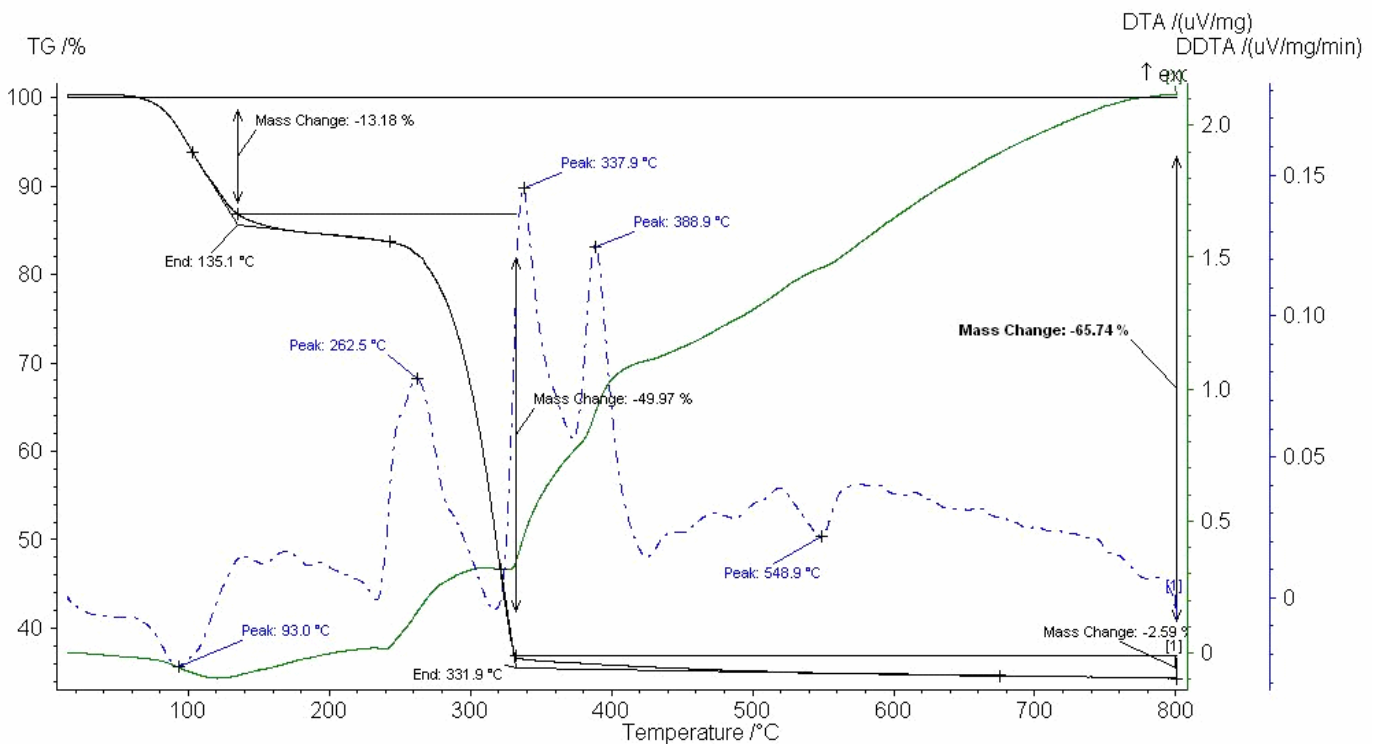


Figure IV.9. TG and DTA curve of $Zn_{0.95}Co_{0.05}O$ xerogel powder which were dried at room temperature.

Cong and his co-workers analyzed DTA and TG curves of $Zn_{(1-x)}Co_{(x)}O$. They reported the thermal decomposition of the oxalate precursors in two steps: first step was from 142-174 °C and the mass loss was calculated as 19.04% and the second step occurred at 386 °C and a mass loss of 38.63 % was calculated. This was due to the decomposition of anhydrous oxalate precursor and the formation of $Zn_{(1-x)}Co_{(x)}O$ [11].

PART V

V.CONCLUDING REMARKS AND RECOMMENDATIONS

$Zn_{(1-x)}Co_{(x)}O$ thin films were coated on glass substrates by using sol-gel deep coating system. The thickness of the film coating increases by increasing the number and solution density. Dense, crack-free and thin sol-gel coating was produced. Co doped ZnO films were observed to be uniform on the glass substrate by using SEM and AFM. X-Ray analysis showed that no secondary phase or metallic Co clusters are found in the material which indicates that, the wurtzite structure may not be affected due to the substitution of cobalt. The analysis of the magnetization measurements indicates that $Zn_{(1-x)}Co_{(x)}O$ films with the Co concentration of 0.25 exhibit ferromagnetism at 305 K.

In addition to these, the temperature changes during the reactions of coated films in DTA show the ferromagnetic behavior as it was found in other measurements.

REFERENCES

- [1] Robert. O’Handley.: “*Modern Magnetic Materials, Principles and Applications*”, Massachusetts Institute of Technology, John Wiley Sons, Inc. (2000) 436
- [2] Jiles, D.: “*Introduction to the Electronic Properties of Materials*”, 2nd Edition, Ames Laboratory, US Department of Energy and Department of Materials Science and Engineering and Department of Electrical and Computer Engineering Iowa State University, (1994) 202.
- [3] Callister, W.D.: “*Materials Science and Engineering an Introduction*”, 5th Edition, the University of Utah, John Wiley Sons, Inc.
- [4] Cullity, B.D.: “*Introduction to Magnetic Materials*”, University of Notre Dame, Addison-Wesley Publishing Company, (1972) 156.
- [5] Science Highlights, The Advanced Light Source
http://www-als.lbl.gov/als/science/csi_archive/137xmcd.html
- [6] Ivanov, V.A.; Ugolkava, E.A.; Pashkova, O.N.; Sanygin, V.P.; Padalko, A.G.: “Ferromagnetism in Dilute Magnetic Semiconductors and New Materials for Spintronics”, *Journal of Magnetism and Magnetic Materials*, 300(2006) e32
- [7] Racheva, T.M.; Critchlow, G.W.: “SnO₂ thin films prepared by the sol-gel process”, *Thin Solid Films*, 292 (1997) 299
- [8] Ayoub, J.P.; Favre, L.; Ronda, A.; Barbezier, I.; Padova, P.De.; Oliveri, B.: “Structural and magnetic properties of GeMn diluted magnetic semiconductor” *Materials Science in Semiconductor Processing*, 9, (2006) 832-835
- [9] Xu, W.; Zhou, Y.; Zhang, X.; Chen, D.; Xie, Y.; Liu, T.; Yan, W.; Wei, S.: “Local structures of Mn in dilute magnetic semiconductor ZnMnO” *Solid State Communications*, 141, (2007) 374-377

- [10] Quesada, A.; Garcia, M.A.; Crespo, P.; Hernando, A.: “Materials for spintronics: Room temperature ferromagnetism in Zn-Mn-O interfaces”, *Journal of Magnetism and Magnetic Materials*, 304, **(2006)** 75-78
- [11] Cong, C.J.; Hong, J.; Zhang, K.: “Effect of atmosphere on the magnetic properties of the Co-doped ZnO magnetic semiconductors” *Materials Chemistry and Physics* **(2008)**
- [12] Zhou, X, et al.: “Effect of Thermal treatment on room temperature ferromagnetism in Co-doped ZnO powders”, *Physica B*, 403, **(2008)**, 3336-3339.
- [13] Agrawal, M.: “Magnetic Properties of Materials, Dilute Magnetic Semiconductors”,
http://www.stanford.edu/mukul/tutorials/Quantum_Optics.pdf
- [14] Das, G.P.; Rao, B. K.; Jena, P.; Kawazoe, Y.; Das, G.P.; Rao, B. K.; Jena, P.; Kawazoe, Y.: “Dilute Magnetic III-V Semiconductor Spintronics Materials: A first Principles Approach”, *Computational Materials Science*, 36 **(2006)** 84.
- [15] Hori, H.; Sonado, S.; Sasaki, T.; Yamamoto, Y.; Shimizu, S.; Suga, K.; Kindo, K.: “High-Tc Ferromagnetism in Diluted Magnetic Semiconducting GaN: Mn Films”, *Physica E*, 324 **(2002)** 142
- [16] Ivanov, V.A.; Krstajic, P.M.; Peeters, F.M.; Fleurow, V.; Kikoin, K.: “On The Nature of Ferromagnetism in Dilute Magnetic Semiconductors: GaAs:Mn and GaP:Mn”, *Journal Of Magnetism and Magnetic Materials*, 258-259 **(2003)** 237
- [17] Dietl, T.: “Dilute Magnetic Semiconductors Functional Ferromagnets” *Polish Academy Of Science, Nature Publishing Group*, **(2003)**
- [18] Dietl, T.; Ohno, H.: “Engineering Magnetism in Semiconductors” *Materials Today*, Volume 6, **(2006)**
- [19] Ohno, H.; Matsukura, F.; Shen, A.; Sugawara, Y.; Akiba, N.; Kuroiwa, T.: “Ferromagnetic (Ga, Mn) As and its Heterostructures”, *Physica E*, 2 **(1998)** 904

- [20] Fitzgerald, C.B.; Vankatesan, M.; Lunney, J.G.; Dorneles, L.S.; Coey, J.M.D.: “Cobalt Doped ZnO a room temperature Dilute Magnetic Semiconductor”, *Applied Surface Science*, 247 (2005) 493
- [21] Pan, F.; Song, C.; Liu, X.; Yang, Y.; Zeng, F.: “Ferromagnetism and possible application in spintronics of transition-metal-doped ZnO films” *Materials Science and Engineering*, R62 (2008) 1-35
- [22] Wang, Y.; Song, Y.; Yin, S.; Yu, G.; Miao, J.; Yuan, S.: “ Ferrimagnetism in Manganese and Cobalt Co-doped ZnO Bulk Samples”, *Materials Science and Engineering B*, 131 (2006) 9
- [23] Peiteado, M.; Iglesias, Y.; Fernandez, J.F.; Frutos, J.; Caballero, A.C.: “Microstructural Development of tin-doped ZnO bulk ceramics”, *Materials Chemistry and Physics*, 101 (2007) 1
- [24] Maensiri, S.; Laokul, P.; Phokha, S.: “A simple synthesis and magnetic behavior of nanocrystalline $Zn_{0.9}Co_{0.1}O$ powders by using Zn and Co acetates and polyvinyl pyrrolidone as precursors”, *Journal of Magnetism and Magnetic Materials*, 381-387 (2006) 305
- [25] Ueda, K.; Tabata, H.; Kawai, T.: “Magnetic and electric properties of transition-metal-doped ZnO films”, *Applied Physics Letter*, Volume 79, (2001) 987
- [26] Fukumura, T.; Jin, Z.; Ohtomo, A.; Koinuma, H.; Kawasaki, M.: “An oxide-diluted magnetic semiconductor: Mn-doped ZnO”, *Applied Physics Letter*, Volume 75, (1999) 3365
- [27] Pearton, S.J.; Abernathy, C.R.; Thaler, G.T.; Fraizer, R.; Ren, F.; Hebard, A.F.; Park, Y.D.; Norton, D.P.; Tang, W.; Stavola, M.; Zavada, J.M.; Wilson, R.G.: “Effects of defects and doping on wide band gap ferromagnetic semiconductors”, *Physica B*, 340-342, (2003) 39-47
- [28] Tiwari, A.; Jin, C.; Kvit, A.; Kumar, D.; Muth, J.F.; Narayan, J.: “Structural, optical and magnetic properties of diluted magnetic semiconducting $Zn_{1-x}Mn_xO$ films” *Solid State Communications*, 121, (2002) 371-374

- [29] Castle, K.: Sol-gel Materials and Nanotechnology, Center of Excellence, www.sgmnm.immt.pwr.wroc.pl/index
- [30] Cullity, B.D.: “*Elements of X-ray Diffraction*”, 2nd Edition, Addison Wesley Publishing Company, Inc. (1978)
- [31] Wikipedia, the Free Encyclopedia,
http://en.wikipedia.org/wiki/Scanning_electron_microscope#References
- [32] Radiological and Environmental Management, Purdue University,
<http://www.purdue.edu/REM/rs/sem.htm>
- [33] Lakshmi, Y.K.; Srinivas, K.; Sreedhar, B.; Raja, M.; Vithal, M.; Reddy, P.: ”Structural, optical and magnetic properties of nanocrystalline Zn_{0.9}Co_{0.1}O-based diluted magnetic semiconductors” *Materials Chemistry and Physics*, (2008)
- [34] Guo, S.; Zhang, X.; Huang, Y.; Li, Y.; Du, Z.: “Investigation on electronic structures nature of charge-transfer transition of ZnO:Co with variation of Co content ” *Chemical Physics letter*, 459 (2008) 82-84
- [35] Chambers, S.A.: “Ferromagnetism in doped thin-film oxide and nitride semiconductors and dielectrics” *Surface Science Reports*, 61, (2006) 345-381
- [36] An, S.Y.; Lee, A.W.; Lee, S.W.; Kim, C.S.: “Magnetic properties of Ba_{1-x}Sr_xFe₁₂O₁₉ grown by a sol-gel method” *Journal of Magnetism and Magnetic Materials*, 242-245, (2002) 413-415
- [37] Arda L., et al.: “Preparation, growth, and magnetic properties of nonvacuum Co doped ZnO powders and films on glass substrate” *Journal of optoelectronics and advanced materials*, *Article in Press*, (2008)
- [38] Belghazi, Y., et al.: “Elaboration and characterization of Co-doped ZnO thin films deposited by spray pyrolysis technique” *Microelectronics Journal*, *Article in Press*, (2008)

BIBLIOGRAPHY

MÜNEVVER ÇAKIROĞLU

Mithatpaşa Cd. Çakmak Mh. Kanaat Sk. No : 18/8 Onur Apt 34770 ÜMRANIYE / İSTANBUL

Home: (216) 3440806, Cell: (532) 6306634
E-mail: bayazitli81@yahoo.com

PERSONAL INFORMATION

Nationality: T.C.

Birth Place: İstanbul

Birth Date: 27.05.81

Marital Status: Married

Driving License: B

EDUCATIONAL INFORMATION

2005 – 2000: Marmara University, Materials Science Engineering

1999 – 1995: Haydarpaşa High School

1991 – 1986: 23 Nisan İlkokulu

PROJECT AND PRACTICES

2003 Summer Course THY Bakım, Destek ve Onarım – Tahribatsız Muayene (NDT-NoneDestructiveTesting)

2004 Summer Course Trakya Şişecam Cam Elyaf Fabrikası – Glass Fiber Production and Stocking

2003 – 2004 Ceramic Materials 3d modeling – Diamond

Final Project / Diffusion Properties of Materials and Finding the Diffusion Coefficient

FOREIGN LANGUAGE

English: Reading: Advanced / Understanding: Advanced /
Speaking: Advanced / Writing: Advanced

COMPUTER KNOWLEDGE

Microsoft Office Applications; Excel, Word, PowerPoint; Internet

CERTIFICATES & AWARDS

Marmara Un. Metal. and Material Eng. First Graduation Degree 26 JUNE 2005
Airport Passenger Services 1 & 2 / THY Training Center 30 NOVEMBER 2005
Troya Check In Certificate / THY Training Center 13 DECEMBER 2005
Civil Aviation Safety /S.Gökçen Eğitim & Araştırma Birimi 19 DECEMBER 2005
Dangerous Goods Regulations / THY Training Center 19 JUNE 2007

WORK EXPERIENCE

- HEAŞ - Havaalanı İşletme ve Havacılık Endüstrileri A.Ş. / Yolcu Hizm. Memuru 10.11.2005 – 01.05.2008
- ANEL El. Pro. Taah. A.Ş. / DCC Engineer 10.10.2008 -